Università degli Studi di Ferrara

DOTTORATO DI RICERCA IN
SCIENZE DELL'INGEGNERIA

CICLO *XXI*

COORDINATORE Prof. STEFANO TRILLO

CORRELATION BETWEEN MICROSTRUCTURAL AND MECHANICAL PROPERTIES OF ALUMINUM ALLOY CASTINGS PRODUCED BY DIFFERENT FOUNDRY PROCESSES

Settore Scientifico Disciplinare ING-IND/21

Dottorando
Dott. MERLIN MATTIA

Tutore
Prof. GARAGNANI GIAN LUCA

_____ _____

Anni 2006/2008

To my parents

"***Research is the art of seeing what everyone else has seen,***
and doing what no-one else has done"
Anonymous

PREFACE

The research activity that I carried out during my PhD is the result of three years of full-time study at the University of Ferrara, Italy, from January 2006 to December 2008. The research and experimental work were performed at the Engineering Department (ENDIF) in Ferrara, with Professor Gian Luca Garagnani being my main supervisor.
The central focus of my PhD was the study of the metallurgical and mechanical properties of aluminum foundry alloys, in particular aluminum-silicon casting alloys. Throughout the three-year period of my PhD, the results were published or submitted for publication in national and international conference proceedings, as well as in national and international journals.

The majority of my work is here presented as a collection of four articles, dealing with different aspects of aluminum castings. The papers included in this thesis are reported in the same format in which they were published or submitted for publication. Each paper is an individual piece of work with separate abstract, introduction, procedure, results and discussion, conclusions and reference sections.
The Introduction of this thesis is intended to provide a summary of the main aims of the articles and the principal conclusions obtained.

The manuscripts are:

Article 1

M. MERLIN, G. TIMELLI, F. BONOLLO, G. L. GARAGNANI, "**Impact behavior of A356 alloy for low pressure die casting automotive wheels**", J. Mater. Process. Technol., 2009, **209**, 1060-1073.

Article 2

M. MERLIN, L. PIVETTI, G. L. GARAGNANI, "**Effect of eutectic modification and the solidification rate on the impact strength of A356 aluminum-silicon alloys**", Metal. Sci. Tech., 2008, **26-1**, 22-29.

Article 3

M. MERLIN, G. L. GARAGNANI, "**Mechanical and microstructural characterization of A356 castings realised with full and empty cores**", Submitted for publication in Metal. Sci. Tech., 2008.

Article 4

S. FERLINI, A. MORRI, E. FERRI, M. MERLIN, G. GIACOMOZZI, "**Effect of silicon particles and roughness on the surface treatments of cast aluminum alloys**", Presented at 3rd International Conference High Tech Die Casting, Vicenza, Italy, September 21-22, 2006.

Moreover, during my PhD I also dealt with the analysis of the main properties of different innovative alloys. A summary of the other research work and publications, developed during the period of my doctoral studies but not explicitly included in this thesis, is reported below:

a. COPPER ALLOYS

The microstructural characterisation of copper alloy welded joints, obtained by different brazing processes, was carried out. In particular, analysis was performed on Cu-Ni-Zn ternary alloys (nickel silver), traditionally used in the glasses branch industry. The two different brazing processes, compared in this research activity, were induction and laser welding. In laser welding, the effects of process parameters

variation, concerning both the laser beam (power and time impact) and the initial conditions of the material surface (presence or absence of surface oxide layer), were evaluated. The results were published in:

M. MERLIN, I. CREPALDI, G.L. GARAGNANI, L. TREBBI, "**Influenza dei parametri del processo di brasatura sulle caratteristiche microstrutturali di giunti in leghe di rame**", Rivista Italiana della Saldatura, IIS, Genova, 2008, **2**, 217-227.

In another activity, hot-tear tests were performed on copper-base casting alloys for artistic applications and the research was carried out as part of "Bronzart - EUREKA PROJECT E! 2210-Eurocare", in order to optimize the functional and aesthetic properties of these alloys. Different types of alloys were produced with the aim of studying the effects of various alloy elements on material properties and to possibly guarantee a better behaviour than that of traditional alloys. A modified Couture-Edwards "dog-bone" test was chosen, because of the easy casting procedure and the hot cracks evaluation, induced by the geometrical parameters. The main results are reported in:

M. MERLIN, G.L. GARAGNANI, G. VENTURI PAGANI CESA, "**Valutazione della resistenza alla criccabilità a caldo di bronzi per applicazioni artistiche**", La Metallurgia Italiana, Milano, 2007, **7/8**, 35-44.

b. HSLA STEELS

Micro-alloyed steels are known to exhibit superior mechanical properties through controlled rolling and specific thermo-mechanical treatments. Steel strength directly comes from a controlled precipitation process of carbides, nitrides and carbon-nitrides formed during the thermo-mechanical treatment, which are responsible for the

fine-grained ferritic structure. Four different micro-alloyed, low-carbon steels were studied: one baseline steel containing a small fraction of Al and N, and the other three with different fraction of Nb and V. Two thermo-mechanical treatments, which differed in the $\gamma \rightarrow \alpha$ transformation temperature, were evaluated. Micro-strengthening contributions of the carbon-nitrides were determined using the Ashby-Orowan approach on the basis of TEM characterisation. Moreover, fatigue tests and fractographic analysis on the fracture surfaces by SEM characterisation were performed. These research projects were published in an international journal and presented at a national congress:

M. CABIBBO, A. FABRIZI, M. MERLIN, G.L. GARAGNANI, "**Effect of thermo-mechanical treatments on the microstructure of micro-alloyed low-carbon steels**", J. Mater. Sci., 2008, **43**, 6857-6865.

M. MERLIN, S. BALDO, G.L. GARAGNANI, "**Effetto degli elementi microalliganti Nb e V sulle proprietà microstrutturali e meccaniche di acciai HSLA da stampaggio**", Presented at 32° Convegno Nazionale AIM, Ferrara, Italy, September 24-25-26, 2008.

c. Ni-Ti ALLOYS

Ni-Ti shape memory alloys (SMAs) show attractive functional properties for a number of engineering and medical applications. The influence of thermo-mechanical treatments on Ni-Ti shape memory strips were studied by means of Differential Scanning Calorimetry (DSC) and Dynamic Mechanical Thermal Analysis (DMTA). DSC analysis is often used to determine transformation temperatures, while DMTA analysis is less used for this kind of materials. The Ni-Ti strips were subjected to cycles of annealing heat treatments, cold deformations and high cooling rates from different quenching

temperatures, in order to control the shape memory effect. The DSC and DMTA results were compared. Moreover, research was carried out in order to investigate the effect of mechanical, chemical and physical parameters on the adhesion between Ni-Ti wires and polymeric materials. Shape memory alloy strips and wires were used to realise the first active deformable structures. A patent was published and two papers were also presented at international and national congresses:

M. MERLIN, G. ROSATI, "**Ventola a geometria variabile e procedimento per la fabbricazione delle relative pale**", Patent n°2008A000013, January 9, 2008.

M. MERLIN, "**Using NiTi shape memory alloy wire for the geometry active control in a cooling fan**", Second Euromediterranean Symposium on Advances Geomaterials and Structures, AGS'08, 2008, **1**, 51-61.

M. MERLIN, M. SCOPONI, "**Studio dell'influenza dei trattamenti termomeccanici sulle temperature di trasformazione di lamine in lega Ti-Ni**", Presented at 32° Convegno Nazionale AIM, Ferrara, Italy, September 24-25-26, 2008.

In addition, another important role of my PhD was to supervise the following M.S. theses, performed at the Engineering Department of the University of Ferrara:

1. Elena Capatti (2006), "**Studio delle caratteristiche microstrutturali e valutazione della resistenza ad impatto della lega A356-T6 per cerchioni automobilistici**". Supervisors: G.L. Garagnani, M. Merlin.
2. Ilaria Crepaldi (2006), "**Valutazione di metodologie innovative di giunzione di componenti per occhialeria**". Supervisors: G.L. Garagnani, M. Merlin.

3. Claudio Maestri (2006), "**Studio delle caratteristiche microstrutturali e valutazione della resistenza ad impatto di leghe di alluminio per componenti motociclistici**". Supervisors: G.L. Garagnani, M. Merlin.
4. Paolo Camanzi (2006), "**Impiego di protossido di azoto nel trattamento termochimico di nitrurazione gassosa. Studio dei parametri produttivi e caratterizzazione metallurgica**". Supervisors: G.L. Garagnani, M. Merlin.
5. Chiara Mingotti (2007), "**Caratterizzazione microstrutturale e analisi termica di formelle in bronzo della Porta del Paradiso del Battistero di San Giovanni e di leghe per applicazioni artistiche**". Supervisors: G.L. Garagnani, M. Merlin.
6. Chiara Menegatti (2007), "**Caratterizzazione microstrutturale e analisi TEM di acciai basso-legati ad elevato limite di snervamento (HSLA)**". Supervisors: G.L. Garagnani, M. Merlin.
7. Martina Scoponi (2007), "**Caratterizzazione meccanica di leghe a memoria di forma pre la realizzazione di un composito funzionale a matrice epossidica**". Supervisors: G.L. Garagnani, M. Merlin, F. Mollica.
8. Marco Bonamici (2007), "**Influenza dei parametri di saldatura sulle proprietà microstrutturali e meccaniche dell'acciaio inossidabile duplex S31803**". Supervisors: G.L. Garagnani, M. Merlin.
9. Silvia Baldo (2007), "**Caratterizzazione microstrutturale e meccanica di acciai da stampaggio basso legati ad alto limite di snervamento**". Supervisors: G.L. Garagnani, M. Merlin.
10. Chiara Soffritti (2007), "**Valutazione della migrazione degli elementi superficiali in funzione dei processi di lavorazione di manufatti prodotti con tecnologia MIM**". Supervisors: G.L. Garagnani, F. Zucchi, M. Merlin, R. Lazzarini.
11. Ermanno Fogli (2007), "**Caratterizzazione dell'interfaccia tra fili in lega a memoria di forma e resina termoindurente mediante prove**

di pull-out e analisi SEM in situ". Supervisors: G.L. Garagnani, M. Merlin.

12. Matteo Zuffi (2008), "**Studio delle caratteristiche microstrutturali e delle proprietà ad impatto dell'acciaio duplex SAF 2205 saldato mediante tecnologia SAW**". Supervisors: G.L. Garagnani, M. Merlin, C. Soffritti.
13. Stefano Succi (2008), "**Caratterizzazione microstrutturale e meccanica di getti motociclistici in lega A356-T6 realizzati con anima piena ed anima cava**". Supervisors: G.L. Garagnani, M. Merlin, C. Soffritti.
14. Laura Renesto (2008), "**Caratterizzazione di leghe a memoria di forma tramite tecnica DSC e prove di Pull-Out**". Supervisors: G.L. Garagnani, M. Merlin, M. Scoponi.
15. Raffaele Balugani (2008), "**Modellazione del comportamento meccanico di fili in lega a memoria di forma con applicazione a compositi funzionali**". Supervisors: R. Rizzoni, M. Merlin.

Other publications:

P. CAMANZI, M. MERLIN, G.L. GARAGNANI, "**Impiego di protossido d'azoto nel trattamento termochimico di nitrurazione gassosa: studio dei processi produttivi e caratterizzazione metallurgica**", La Metallurgia Italiana, Honegger, Milano, 2009 (in press).

M. MERLIN, L. PIVETTI, G. L. GARAGNANI, "**Influenza del trattamento termico e delle caratteristiche microstrutturali sulla resilienza della lega di alluminio A356 colata in conchiglia**", Presented at 32° Convegno Nazionale AIM, Ferrara, Italy, September 24-25-26, 2008.

A. RIGHINI, M. MERLIN, P.L. ANTONA, G.L. GARAGNANI, "**Carbocementazione e tempra di ruote dentate – Valutazioni dimensionali e microstrutturali**", Presented at 32° Convegno Nazionale AIM, Ferrara, Italy, September 24-25-26, 2008.

G.L. GARAGNANI, M. MERLIN, E. MELLO, S. SIANO, "**Caratterizzazione metallurgica delle formelle bronzee della 'Porta del Paradiso' del Battistero di Firenze: indagini preliminari**", Proceedings of IV Convegno Nazionale AIAR, Patron Editore, Bologna, 2007, 599-618.

M. MERLIN, E. FERRI, "**Evolution of welding techniques for metal matrix composite materials**", A&L, Edimet, Brescia, Italy, 2007, **4**, 104-110.

G.L. GARAGNANI, F. BONOLLO, F. PIASENTINI, M. MERLIN, G. TIMELLI, "**Influence of microstructure and casting parameters on the impact strength of low-pressure A-356 aluminium alloy for car wheels**", Presented at 3rd International Conference High Tech Die Casting, Vicenza, Italy, September 21-22, 2006.

M. MERLIN, E. FERRI, "**Prove 'charpy' per getti migliori**", Alumotive, Edimet, 2006, **2**, 112-118.

ACKNOWLEDGEMENTS

I wish to thank all the people I have worked with during these three years of my PhD.

I would especially like to thank my supervisor Prof Gian Luca Garagnani for proposing this PhD research project to me three years ago and for his advice, guidance and for sharing his expert knowledge with me.

I wish to acknowledge the encouragement and cooperation of my family and a number of friends.

How can I ever forget the help and the wonderful times spent together with my friends and colleagues of Office 027? Thank you Gianluca, Angelo, Valerio, Mauro, Emiliano and Alessandro.

Most of all I would like to thank Alice, for her love, patience and understanding.

ABSTRACT

Aluminum is quite a new material and the production of aluminum-alloy castings has greatly increased in the last recent years. Nowadays, there is a continuous market requirement to produce lighter vehicles and to increase fuel efficiency, therefore roughly two thirds of all aluminum castings production is within the automotive field. Even though the applications of aluminum in this scenario are considerable, some aspects affecting the quality and the soundness of cast products are still not fully understood. The aim of the research work presented in this PhD thesis was to study the correlation between mechanical and microstructural properties of Al-Si castings, in order to contribute to fill this lack of knowledge. The majority of my research work is included here as a collection of four papers submitted in the form they were published or submitted for publication. Each paper is a stand-alone work with separate abstract, introduction, experimental procedure, results, conclusions and reference sections. Different kinds of automotive and motorcycle structural components, realised by means of low pressure die casting and permanent mould gravity casting, and experimental components realised by sand mould casting were produced and studied. Impact strength and tensile strength tests were performed in order to understand the correlation between microstructural and mechanical properties better. The effect of different cooling rates, eutectic modification, defects, heat treatments and type of cores was studied with the aim to improve the design of aluminum alloy structural components. Moreover, the effect of the eutectic microstructure on the anodizing surface treatment in aluminum-silicon alloys was studied. The influence of silicon content, morphology and distribution of the eutectic phase on the anodizing process was investigated on both sand-cast and die-cast samples.

Different techniques for the microstructural examination were employed in the research study; Optical Microscopes (OM) and Scanning Electron Microscopes (SEM) with Energy Dispersive X-ray (EDS) microprobe were used and also X-ray investigations were carried out to verify the presence or the absence of porosities and defects in the castings. In addition, numerical simulations were carried out and the results were compared with those obtained by microscopy. In terms of utility, the numerical simulations were able to predict the formation of macro-defects and the final scale of microstructure within the castings, confirming their potential as an engineering tool for predicting microstructural and mechanical properties throughout the castings.

SOMMARIO

L'alluminio è un materiale abbastanza nuovo e la produzione di getti in lega di alluminio è aumentata notevolmente negli ultimi anni. Oggigiorno il mercato richiede continuamente la realizzazione di veicoli più leggeri e con minori consumi di carburante, pertanto quasi due terzi della produzione di getti di alluminio è rivolta al settore automobilistico. Nonostante il fatto che l'applicazione dell'alluminio in questo settore sia considerevole, alcuni aspetti riguardanti la qualità e l'integrità dei getti non sono ancora completamente noti. Lo scopo dell'attività di ricerca presentato in questa tesi di dottorato è stato lo studio della correlazione tra proprietà meccaniche e microstrutturali di getti Al-Si per contribuire a supplire a queste lacune. Il lavoro di tesi è presentato come collezione di quattro articoli, nella stessa forma in cui sono stati pubblicati o inviati per la pubblicazione. Ogni articolo include riassunto, introduzione, procedura sperimentale, risultati, conclusioni e riferimenti bibliografici. L'attività ha riguardato lo studio di componenti strutturali di impiego automobilistico e motociclistico, prodotti mediante colata in bassa pressione e colata per gravità in conchiglia, nonché di getti sperimentali colati in sabbia. Sono state effettuate prove di resilienza strumentata e prove di trazione al fine di individuare delle correlazioni sempre più approfondite tra microstruttura e proprietà meccaniche. In particolare, è stato valutato l'effetto di diverse velocità di solidificazione, di differenti trattamenti di modifica, dei difetti, del trattamento termico e del tipo di anime, con lo scopo di garantire una progettazione sempre più efficace. Inoltre, è stato studiato l'effetto della microstruttura sul trattamento di anodizzazione delle leghe alluminio-silicio. L'indagine è stata effettuata su campioni colati in sabbia e pressocolati, valutando l'influenza del contenuto di silicio e della morfologia e distribuzione dell'eutettico.

Per effettuare le analisi microstrutturali sono state utilizzate tecniche di microscopia ottica (MO) ed elettronica in scansione (SEM) con microsonda EDS; indagini ai raggi X hanno consentito di verificare la presenza o l'assenza di porosità e difettosità nei getti. Inoltre, a sostegno dell'attività di ricerca sono state eseguite anche delle simulazioni numeriche dei processi di colata e i risultati sono stati confrontati con quelli ottenuti mediante microscopia. Le simulazioni numeriche si sono dimostrate in grado di predire la scala microstrutturale e la formazione di macro-difetti, confermando il loro potenziale come strumento ingegneristico per la previsione delle proprietà meccaniche e microstrutturali dei getti.

TABLE OF CONTENTS

INTRODUCTION

Aluminum is the most widely used non-ferrous metal and its global production exceeds that of any other metal except iron. It can be cast by all of the processes used in casting metals. The three main processes, in increasing order of production quantities are sand casting, permanent mould casting and die casting. Other casting processes include investment casting, lost foam casting, ceramic moulding, plaster moulding, and the new squeeze casting and semi-solid casting.

Economic considerations, technical limitations and quality requirements determine the choice of a casting process. As far as the economical and technical aspects are concerned, the size, the number and the design features of the castings are important factors in the selection of the casting method. Instead, the quality of a casting refers to both its soundness (freedom from surface defects, porosity, cracks) and the expected mechanical properties (strength and ductility).

The research activity that I carried out during my PhD and the main objectives of this thesis are to provide a contribution to the knowledge of the influence of the microstructural aspects on the quality of aluminum alloy castings. Aluminum-silicon castings constitute 85% to 90% of the total aluminum-cast parts produced; aluminum alloys containing silicon as the major alloying element offer excellent castability, good corrosion resistance, and can be machined and welded. For these reasons, EN AC-42100, EN AC-43100 and EN AC-46100 alloys have been analysed.

Different aspects of the processing and process parameters were studied and the main results are here presented as a collection of articles:

- The aim of Article 1 was to study the impact behaviour of KV sub-size Charpy samples drawn from A356 aluminum alloy 17-inch

wheels, produced by a low pressure die casting process. The wheels showed different geometry and thermal treatment. In this paper the effects of microstructure and defects on the impact properties were studied. Numerical simulations were performed to study the filling and the solidification behaviour of the alloy of the wheels analysed, in order to predict the final microstructure and shrinkage formation.

- The aim of Article 2 was to study the impact properties of Charpy specimens machined from cast plates produced in sand moulds. Unmodified, sodium-modified and strontium-modified castings were tested; the addition of small amounts of modifying elements to the molten metal causes the eutectic silicon to solidify with a fine, apparently globular, morphology. In this paper the effects of eutectic modification and of the cooling rate on the impact properties were studied. The fracture profile and surface of cracked samples were analysed by means of Optical and Scanning Electron Microscopes, in order to investigate the effect of eutectic silicon and intermetallic particles. Numerical simulations were carried out to study the filling and the solidification behaviour of the sand-cast plates under different cooling conditions, to be compared with the real ones.

- The aim of Article 3 was to study the effect of replacing full cores with empty cores for producing automotive components by means of the permanent mould casting technique. The use of full cores allows good castings to be obtained with a low level of defects. Nevertheless, an extra phase of the production cycle is necessary to have an optimal emptying of the internal cavities of the castings, with an increase in costs. The component analysed was one of the three parts of a motorcycle frame, realised in aluminum alloy A356 and T6 heat-treated. In this paper tensile strength tests were performed on samples drawn from four different zones, in order to compare the mechanical and microstructural properties of the

castings realised with the two different kinds of core. The effects of secondary phases, porosities and morphology and distribution of eutectic silicon particles were considered. Cost, weight and time-cycle reductions in the production of the component, due to the elimination of the extra phase using empty cores, were evaluated.

- The aim of Article 4 was to evaluate the effect of the eutectic microstructure on the anodizing surface treatment in aluminum-silicon alloys. In this paper, the influence of silicon content, morphology and distribution of the eutectic phase on the anodizing process was investigated. EN 42100 and EN 43100 alloy sand-cast samples and EN 46100 alloy die-cast samples were studied. In addition to the silicon effect, the influence of the surface finishing, on the manner in which the oxide develops and its properties, was considered. Each sample was characterised with roughness profiles before and after the anodizing process; then, microstructural characterisation of the coatings were carried out by means of optical and scanning electron microscopes.

From this PhD thesis the following conclusions can be obtained:

- Impact strength tests performed on Charpy V-notch specimens drawn from three different A356 17-inch wheels, produced by low pressure die casting, show interesting correlations between microstructure and impact strength values. A finer microstructure always corresponds to higher impact strength. Impact energy values are lower in the as-cast microstructure than in the T6 heat-treated one. The resistance to crack propagation values is within the range of 60-75% of the total absorbed energy and the highest values are shown by the as-cast microstructure. A direct correlation between the resistance to crack propagation and SDAS is found. The crack crosses the interdendritic eutectic region where the microstructural

analysis reveals microshrinkage porosity, cracked eutectic silicon with different size and morphology in the as-cast and in the T6 heat-treated wheels, the presence of cracked intermetallic particles. Casting defects become critical when concentrated around the V-notch, where they reduce the load bearing area of Charpy specimens. Therefore, the presence of defects is critical on impact properties and can overcome the effect of the microstructure.

- Impact strength tests carried out on plate castings realised by means of sand casting technique reveal that, when the value of the cooling rate is the same, modified samples show higher impact strengths than unmodified ones; in particular, this is due to the change of eutectic silicon particles from acicular to fibrous morphology. This effect is emphasized in strontium-modified samples, where a more uniform distribution of eutectic silicon is found. A direct correlation between the propagation energy and SDAS is only obtained in modified samples, because the scatter of data is too large in unmodified ones. The fracture surface of the samples reveals the interdendritic path of the crack, with the presence of microshrinkage and of Fe-rich intermetallic platelets. Numerical simulations are very useful when evaluating the quality of the casting as a result of the manufacturing cycle; they are able to predict the formation of macro-defects, as indicated by a feeding criterion, and the final scale of microstructure within the casting.

- The analysis of microstructure and mechanical properties of castings, realised with full and empty cores and by means of permanent mould casting technique, shows that SDAS is comparable in corresponding positions for the two kinds of castings. The distribution of eutectic silicon particles is generally uniform and globular. UTSs and YSs are inside the expected range of values; A%s should be increased in the castings realised with empty cores,

probably by means of an optimisation of the heat treatment parameters. In general the mechanical properties of both kinds of castings are comparable. An inverse correlation between UTS and SDAS is obtained; a finer microstructure always corresponds to higher UTSs, while YS does not seem to be well-correlated to the scale of the dendritic structure. In the castings produced with empty cores the extra “hot flogging” heat treatment is not necessary to guarantee the required mechanical and microstructural properties, it can be eliminated and a reduction of 9% in the total production costs is evaluated.

- The silicon content, size and distribution in the eutectic mixture of aluminum-silicon alloys affects the growth of the anodized layer and causes remarkable modifications to the morphology and distribution of the pores present within it. During the anodizing process, the growth of the anodic layer, in particular its thickness, is also affected by the initial roughness of the component. In the EN 42100 alloy, the roughness increases after anodizing process only for low R_a, while for EN 43100 and EN 46100 alloys, where the percentage of silicon increases, the roughness values increase after anodizing process for each level of examined R_a. Sand-cast samples show considerable differences between the oxide thickness depending on the surface roughness, probably due to the large size of the eutectic silicon particles. Instead, the oxide layer has homogeneous thickness in the die-cast EN 46100 alloy samples, where the silicon particles are finely dispersed.

ARTICLES

Article 1

IMPACT BEHAVIOUR OF A356 ALLOY FOR LOW PRESSURE DIE CASTING AUTOMOTIVE WHEELS

Mattia Merlin*, Giulio Timelli**, Franco Bonollo**,
Gian Luca Garagnani*

* Department of Engineering - ENDIF
University of Ferrara
I-44100 Ferrara
Italy

**Department of Management and Engineering - DTG
University of Padova
I-36100 Vicenza
Italy

Journal of Materials Processing Technology, 2009, **209**, 1060-1073

ABSTRACT

Instrumented impact strength tests have been carried out on KV sub-size Charpy samples drawn from A356 aluminium alloy 17-inch wheels, produced by a low pressure die casting. The wheels show different geometry and thermal treatment. In this paper, the effects of microstructure and defects on the impact properties are studied. The results indicate that the impact energy is lower in as cast wheel than in T6 heat treated wheels. A finer microstructure always corresponds to higher impact strength, while a direct correlation between the resistance to crack propagation values and secondary dendrite arm spacing (SDAS) exists. Casting defects, revealed by means of X-ray and density measurements techniques, become critical when concentrated around the V-notch, where they reduce the load bearing area of Charpy specimens. The fracture profile and surface of Charpy specimens have been investigated revealing how the crack crosses the interdendritic eutectic region where a significant fraction of cracked eutectic silicon and intermetallic particles is found.

Numerical simulations have been performed to study the filling and solidification behaviour of the alloy of the wheels analysed, in order to predict the final microstructure and shrinkage formation. Solidification times, estimated by means of SDAS measurements and calculated with a numerical simulation approach, show a good correspondence. Critical areas, as concern hot spots and shrinkage porosities, are generally revealed in the zone of the wheels between the spoke and the rim, as well as in the rim area.

KEYWORDS

Aluminium alloys; impact strength; castings defects; microstructure; numerical simulation.

1. INTRODUCTION

Lowering pollutant emission is a priority objective of international policies together with lowering energy consumption and increasing recycled materials; not only for its effect on the quality and environmental equilibrium, but because it has a strong impact in the competitiveness of companies in several sectors. In this context, only the introduction of technological innovation will be able to reconcile objectives of an environmental and energetic nature with those of a competitive type. Recently, the application of aluminium alloys in automotive sector can be one of these economically sustainable innovations, which enable a wider mix of objectives to be achieved. Both Flinn (1963) and Sicha (1971) affirm in their works that, due to their excellent castability and good compromise between mechanical properties and lightness, aluminium-silicon alloys are the most important and widely used casting alloys in order to cast components with complex shapes.

A consolidated example of aluminium alloy employment regards the production of wheels, which, together with an improved aesthetic appearance, guarantees an improvement of driving, like directed consequence of the inertia reduction of the wheels. These components are somewhat unique as they must meet, or exceed, a combination of requirements, from high quality surface finish, as wheels are one of the prominent cosmetic features of cars, to impact and fatigue performance, because wheels are critical safety components. Generally, the main technology for casting aluminium alloy wheels is the Low Pressure Die Casting (LPDC), which guarantees to obtain a good compromise between high mechanical properties, high production, cost-effectiveness and design demand. Street (1986) stated that LPDC allows to produce castings similar to those obtained by gravity casting, with good superficial aspect and thin thicknesses, but the advantage to have one central metal inlet and the absence of risers allows to obtain an optimal yield, around 85-95%.

Li et al. (2004) analysed the effect of various alloying elements and different heat treatments in A319-type alloys by means of instrumented impact test; in particular they found that impact tests can give a measure of the capability of the material to resist to crash, providing an useful estimation of the ductility of an alloy under conditions of rapid loading. Analysing the impact properties of Al-Si foundry alloys, Paray et al. (2000) evaluated the total absorbed energy of the samples subjected to impact test like the sum of the energy required for crack nucleation and the energy required for crack propagation, in order to describe the dynamic toughness of the material. Srivastava et al (2006) demonstrated that in the case of cast aluminium alloys the presence of a notch can decrease the impact values even further, by up 80%, when compared to un-notched specimens; even a shallow scratch of 0.1 mm reduces the energy absorption by 30%. If a notch is present, the absorbed energy can be dependent on the notch geometry than on the microstructure.

Impact test is a useful methodology in evaluating the effects of process parameters and microstructure on dynamic fracture toughness of engineering materials. Murali et al. (1992) evaluated the influence of magnesium content in the AlSi7Mg0.3 alloy with low iron level: the absorbed energy drops significantly by about 50% with increasing magnesium content from 0.32 wt.% to 0.65 wt.%. Similar behaviour is observed increasing the iron content from 0.2 wt.% to 0.8 wt.%, at 0.32 wt.% Mg, due to an increased precipitation of β-Al_5FeSi platelets. Shivkumar et al. (1994), analysing Charpy specimens in A356-T6 machined from plate and cylindrical castings, demonstrated that the strontium modification, as well as an increase of solidification rate, improves the impact properties of sand and permanent mould castings, even if the effect is more pronounced at low magnesium and iron content.

As specified by Zhang et al. (2002), the T6 heat treatment provides beneficial effects to cast aluminium components: it increases the yield

strength, through the precipitation of a large number of fine β'-Mg_2Si particles, and improves the ductility, through spheroidisation of the eutectic silicon particles. Earlier Càceres et al. (1995) and later Wang and Càceres (1998) observed that the inter-particle spacing plays a dominant role in determining cracks' nucleation and propagation and that the fracture path considerably depends on the dendrite cell size. The nucleation of the cracks usually starts with cracking of brittle particles. Once a large number of particles are cracked, cracks grow by linking microvoids formed by the cracking of these particles. With a smaller inter-particle spacing, the microvoids link and grow easily. Li et al. (2004) demonstrated that oxides, such as phosphorous oxides, which act as nucleation sites for Al_2Cu precipitates in A319-T6 alloy, can accelerate the cracking process reducing the impact properties.

While the benefit effect of T6 heat treatment is recognized, the additional cost and required time are substantial. Zhang et al. (2002) showed that shortening the total time of the T6 heat treatment cycle there exists a region where the impact energy decreases to a minimum before increasing. The cause of this region seems due to a conflict between the negative effect of solution treatment on ductility and impact strength, associated with a rapid increase in the yield strength and the more slowly developing positive effect associated with the spheroidization and coarsening of silicon particles.

The aim of this study is to investigate the impact properties of KV sub-size Charpy specimens, drawn from A356 17-inch wheels with different geometry and temper, by means of instrumented Charpy impact testing including discussion of individual energy portions during fracture. Microstructural features, such as secondary dendrite arm spacing (SDAS) and eutectic silicon particles, have been correlated to impact properties: absorbed energy, maximum load, crack nucleation and propagation energy. Càceres and Selling (1996) carried out a series of experiments to quantify the effect of casting defects in AlSi7Mg0.4-T6 casting alloy and they found that porosity is critical on mechanical

properties of cast aluminium alloys, since it can overcome the effect of microstructure itself. In order to evaluate the presence of porosity, density measurements and X-ray investigations have been carried out on KV samples. In addition to metallographic inspections, fractography has been presented to underline the effect of microconstituents on crack nucleation and propagation. Concurrent with experimental approach, the filling and solidification behaviour of the wheels analysed have been assessed via numerical simulation codes.

2. EXPERIMENTAL PROCEDURE

Instrumented impact tests have been performed on KV sub-size Charpy specimens drawn from different A356 wheels, named wheel-1, -2 and -3 respectively. While wheel-1, a 7-spoke wheel in the as cast temper, has a weight of 10.6 kg, wheels-2 and -3, which are 5-spoke wheels in the same T6 condition, weigh 12.2 and 11.9 kg respectively. The wheels' diameter is 43.35 cm, while the rim width is 21.8 cm for wheel-1 and 19.1 cm for wheels-2 and-3. The wheels differ mainly on the geometry and thickness of spokes and rims. All the wheels were cast by LPDC.

2.1. Alloy and casting parameters

The cast wheels were produced with A356 alloy, an hypoeutectic aluminium-silicon alloy, in the form of ingots, whose composition is indicated in table 1. The material was melted in an electric-induction furnace set up at 750±5°C. The melt was degassed with nitrogen and modified with Sr-containing master alloy. AlTi5B1 rod type grain refiner was also added to the molten metal. A Straube-Pfeiffer test was performed to evaluate the molten quality before casting.

Table 1. Chemical composition of A356 alloys studied in the present work (wt.%).

Alloy	Al	Si	Fe	Cu	Mn	Mg	Zn	Sn	Ni
A356	bal.	7.32	0.147	0.002	0.006	0.30	0.001	0.003	0.005

The die was made by an AISI H11 tool steel, and the die holder was made by a UNI 4010-75 FeG52 (C50) carbon steel. The temperature in the die, measured with thermocouples, was in the range of 450-520 ± 3°C.

The casting process is cyclic and begins with the pressurization of the furnace, which contains a reservoir of molten aluminium. The excess pressure in the holding furnace forces the molten aluminium to fill the die cavity. The casting cycle is divided in the following steps:

- filling the die cavity in 60±4 s up to a final pressure of 0.4±0.015 bar;
- overpressure of 2±0.03 bar, reached after 10±2 s from the end of the filling and applied for 210±5 s;
- discharging the pressure of the furnace in 5±1 s;
- after the complete solidification, the side dies are opened (5±1 s), the top die is raised vertically (10±1 s) and the casting is ejected (5±1 s).
- the die is closed and the cycle restarts.

Typical cycle time is about 6 minutes. During solidification, cooling rates are controlled by forcing air (2-3 bar) through internal channels in the top and bottom dies, at various times during casting cycle. On the side dies, cooling can be ensured by air jets, aimed at various sections of the exterior face. In spite of the different geometry, the wheels were cast with the same casting cycle.

The wheels-2 and -3 were solution treated in an air circulated furnace held at 535±5°C for 6h, quenched in a hot water bath, held at 80°C, and then artificially aged.

2.2. Impact testing

Impact tests were performed on Charpy samples drawn from the spoke and the rim region of the wheels (figure 1). Charpy specimens 5 x 10 x 55 mm and a V-notch of 2 mm depth with a root radius of 0.25 mm were made.

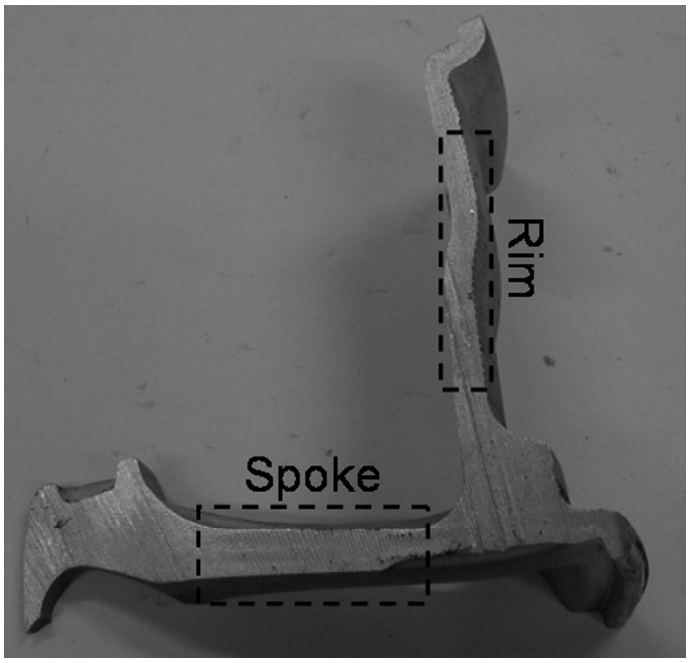

Fig. 1. Position of the spoke and the rim zone in the wheels analysed.

A Ceast instrumented Charpy pendulum, with an available energy of 50 J and an impact velocity of 3.46 m/s, was used. The pendulum impact machine, connected to a data acquisition system, is equipped with an auto-calibration system of the hammer, in order to execute the appropriate adjustments due to pendulum frictions and air resistance. During impact testing the total impact energy (W_t), calculated as the integral of load-displacement curve, and the maximum load (F_m) were measured, as well as the energy at maximum load (W_m) and the crack propagation energy (W_p), i.e. the energy absorbed from the maximum load to the end of test, which is considered when the load comes to 2% of its peak. At the same time, the energy absorption was evaluated through the measurement of the pendulum's angle of rise (mechanical

value, *CV*). W_t and *CV* describe the same phenomena in a different manner. The slight difference between W_t and *CV* was estimated equal to ~0.12 J.

2.3. Porosity measurement and X-ray investigation

In order to obtain a quantitative measure of percentage porosity on the same 5-spoke type wheel, samples taken from wheels-2 and -3 were analysed by means of density measurements. As previously said, these two wheels are 5-spoke wheels in the same T6 condition, differing on the geometry and thickness of the spokes. Every sample was weighted in air and water, and the density calculated according to Archimedes's principle:

$$\frac{W_a}{W_a - W_o}\rho_o = \rho \tag{1}$$

where W_a and W_o are the sample's weights in air and water, ρ_o is the density of water at room temperature and ρ is the experimentally observed density. The percentage porosity was defined by the equation

$$\%Porosity = \frac{\rho_{nom} - \rho}{\rho_{nom}} \times 100 \tag{2}$$

where ρ_{nom} is the density of fully dense material.

In order to localise the porosity distribution around the notch, impact test specimens were analysed with a micro focus X-ray equipment, which can magnify an image several times while still offering a better definition than a conventional X-ray tube. Every wheel was previously mapped throughout with a macro focus X-ray equipment for a preliminary analysis and comparison.

2.4. Image analysis and fractography

The microstructures of the as cast and the T6 heat treated impact test samples were observed using an optical microscope and quantitatively analysed by means of an image analyser. Average SDAS values were obtained using the linear intercept method. In each specimen, drawn from the hub, the spoke and the rim region of the wheels analysed, ten random areas were acquired over the entire sample surface for SDAS analysis. Several measurements were done, in order to obtain reliable mean values.

Important information, concerning fracture path and microstructure components involved in crack process, were obtained observing the fracture profile, on the prepared metallographic section, cut out perpendicularly to the fracture surface. An optical microscope was used for this investigation. Finally, the fracture surfaces of the Charpy specimens after the impact test were observed and analysed by scanning electron microscopy (SEM) and by energy dispersive X-ray spectroscopy (EDS).

2.5. Casting simulation

The MAGMASOFT® v.4.2. (2002) software, with its module for low pressure die casting MAGMAlpdc, was used for numerically simulating the filling and solidification behaviour of analysed wheels. The characteristics of MAGMAlpdc used in this study are as follows:

- ease of physical interpretation of various steps of algorithms;
- conservation of physical properties;
- reduction of solving time.

Basic governing equations of MAGMASOFT® are continuity equation, Navier-Stoke's equation, energy equation and volume of fluid (VOF) method for the free surface movement during the die filling. MAGMAlpdc employs the finite volume approach to convert

differential equations into algebraic ones and solve them on a rectangular grid.

For every wheel, the CAD model was drawn and imported in the simulation software where a Controlled Volume Mesh of 15300000 cells for the whole system (die and casting) was automatically generated by MAGMAlpdc; a mesh of 670000 elements was generated for the die cavity. The initial conditions for numerical simulation were defined to reproduce the LPDC parameters. The pouring temperature was set at 750°C, while, for the die, the temperature for the first cycle was assumed to be at a uniform temperature of 450°C. In the subsequent cycles, the initial temperature in the die is taken to be the predicted temperature distribution at the end of the previous cycle. A number of 15-20 cycles were taken after the start up to reach a quasi-steady state temperature in the die. The thermal conductivity of the die and die holder varied in the range of 33.4-31.5 W/mK and 39.4-35.6 W/mK respectively, in the working temperature range of 450-520°C. The thermal conditioning of the die is given by air circuits or jets at 30°C. The other physical constants and properties of the die and the alloy, and their evolution with temperature, were chosen among those present in the MAGMASOFT® v.4.2. (2002) software database, as well as the heat transfer coefficients (HTC), taking into account affecting parameters, like the type and thickness of coating, and the pouring temperature. To define the whole set of boundary conditions in the model, the process parameters (e.g., regarding the filling and cooling cycle) and the cycle time, acquired from the casting process, were imported in the software, increasing the reliability of numerical simulation. Virtual thermocouples were inserted in the different zones of the die in order to control the temperature profiles and to compare these values with the real ones. Solidification time and feeding properties were assessed via numerical simulation codes, in order to predict the final microstructure and the shrinkage formation.

3. RESULTS AND DISCUSSION

3.1. Microstructural analysis

Impact strength tests can supply useful information on fracture mechanisms of the material under conditions of rapid loading and on the role played by the secondary phase particles and the defects like porosity, oxides and inclusions on crack trigger and propagation, and on fracture morphology.

The microstructure of the wheels analysed consists of a primary phase, α-Al solid solution, and an eutectic mixture of aluminium and silicon. α-Al precipitates from the liquid as the primary phase in the form of dendrites. Intermetallics compounds, such as Fe-rich intermetallics, were also observed.

The scale of microstructure in different zones of the wheels analysed was characterized by means of SDAS measurements and then correlated with impact properties. These data are described in Section 3.2.1.

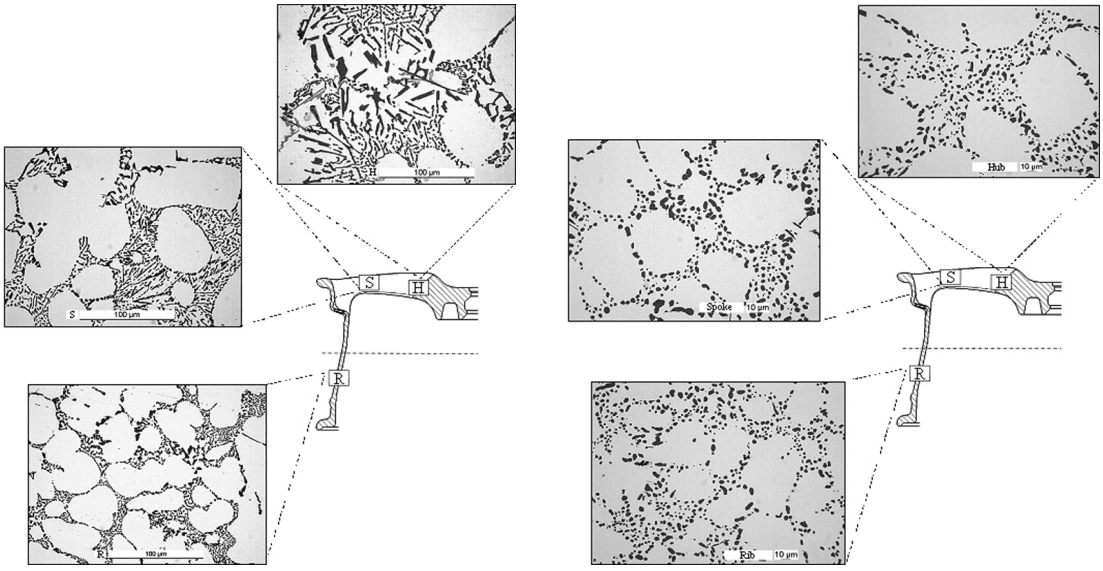

Fig. 2. Microstructure of (a) wheel-1 and (b) wheel-2 with reference to the different positions analysed.

In figure 2, typical microstructures of the wheels analysed are reported with reference to the different positions, in particular the hub (H), the spoke (S) and the rim (R) zones. While figure 2a shows the microstructure of as-cast wheel-1, in figure 2b the microstructure of T6 heat treated wheel-2 is presented.

3.1.1 Microstructural defects and secondary phases

Microshrinkage were found in the spoke and in the rim region of each wheel, while no defects were observed in the hub zone. An example of microshrinkage porosity in the rim area is shown in figure 3.

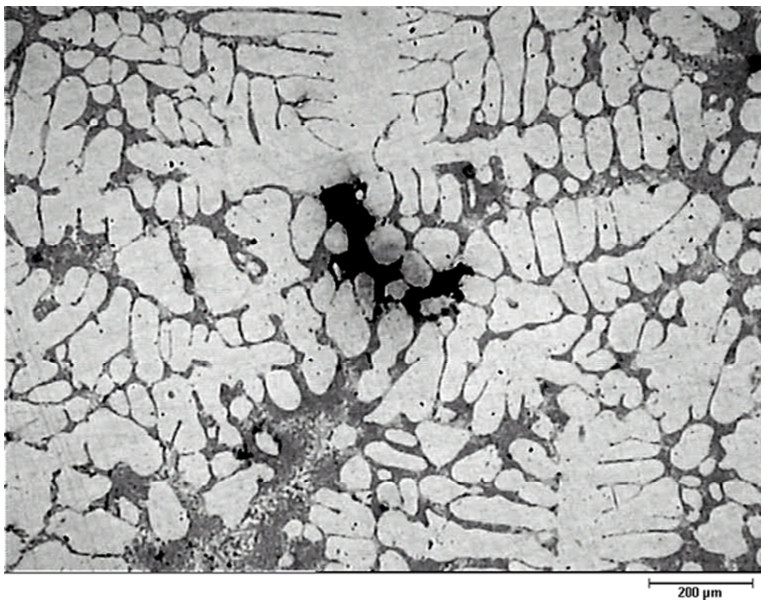

Fig. 3. Optical micrograph of a shrinkage porosity in the rim zone.

Brown (1999) emphasized that the presence of Fe in the alloy involves a loss in ductility, shock resistance and machinability. Secondary phase particles, such as Fe-rich intermetallics with typical needle shape, were observed in the samples analysed. In figure 4 and 5, the presence of secondary phases is evidenced in the specimens drawn from as cast wheel-1 and T6 heat treated wheel-3.

Concerning eutectic silicon, different size and morphology were observed in as cast wheel-1 than in the T6 heat treated wheels, as a consequence of the solution heat treatment. In both wheels-2 and -3, the eutectic silicon is present as well dispersed globules (figure 5). In the as cast wheel, the eutectic silicon is in the form of fibrous particles due to Sr modification (figure 4). Pedersen (1999) showed how fibrous, or better globular, eutectic silicon particles improve the impact properties of cast Al-Si alloys.

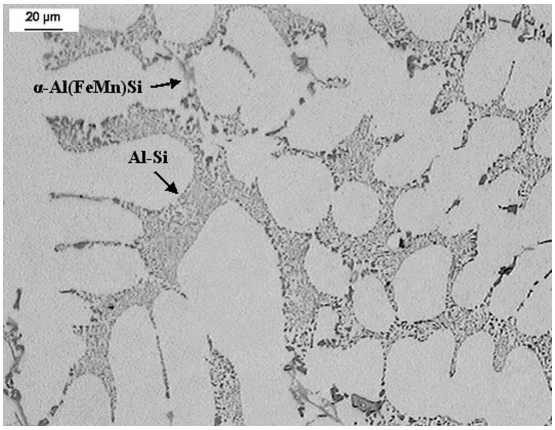

Fig. 4. Optical micrograph showing secondary phase particles in rim area of wheel-1. The eutectic silicon is in the form of fibrous particles in the interdendritic channels.

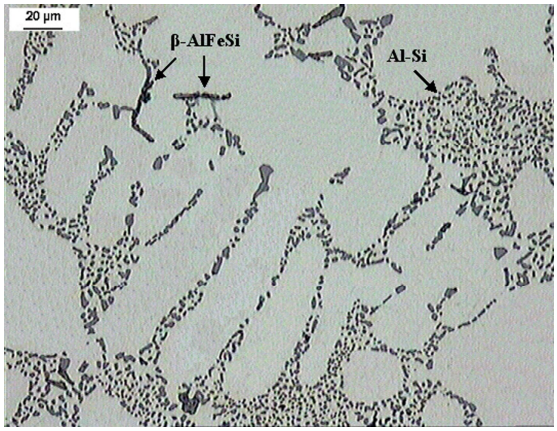

Fig. 5. Optical micrograph showing secondary phase particles in rim area of wheel-3. The distribution of eutectic silicon is homogeneous and globular.

3.2. Impact strength

Figure 6 shows the mean values of the total impact energy, with standard deviations, obtained on sub-size V-notch Charpy sample using the instrumented test method according to UNI EN ISO 14556:2003. The samples drawn from the spoke and the rim zone of as cast wheel-1 showed close impact energies, 1.53 and 1.55 J respectively, with low standard deviation (~0.10 J). In wheel-2, the

impact energy increased from values of 2.24 J in the spoke to 2.55 J in the rim. In wheel-3 the trend and the increase were the same: the specimens drawn from the spoke region revealed lower impact values, 2.41 J against 2.75 J, even if the standard deviation was higher (~0.3 J). The T6 heat treatment influenced the impact properties, increasing the impact energy of the specimens by more than 60%, as evidenced in figure 6.

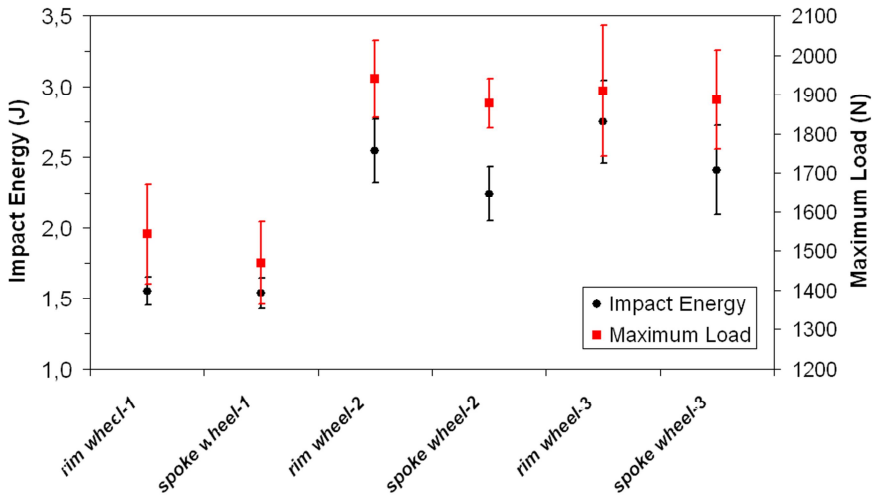

Fig. 6. Impact energy and maximum load measured in the different positions of the wheels. The standard deviations are shown as error bars.

The maximum load values as a function of the position of the specimens taken from the wheels is also shown in figure 6. Comparing the results of the heat treated with the as cast wheels, the T6 heat treatment increases the maximum load of about 26%. In wheel-1, the maximum load increases from 1470 N to 1544 N (about 5%), considering the spoke and the rim region, respectively. Similar trend was observed in wheels-2 and -3, where the maximum load was higher for the specimens drawn from the rim zone. While the value increases of about 3% in wheel-2, the increase is only 1.2% in wheel-3, where the standard deviation is however higher.

Figure 7 shows two load-time curves obtained from the instrumented impact tests. The curves refer to the samples obtained from the region of the spoke and the rim of wheels-1 and -3. Li et al. (2004) showed that the initial fluctuation of the curves is due to the inertial loading of the hammer as a result of the acceleration of the specimen from the remainder. The shape of the load-time curves in figure 7a, similar to that obtained from T6 heat treated wheels (figure 7b), shows rather high values of nucleation and propagation energies. The load values are higher for the specimens drawn from the T6 heat treated wheels, in agreement with the results obtained by Li et al. (2004) and Paray et al. (2000). After the peak force, the slow load reduction indicates a controlled crack propagation.

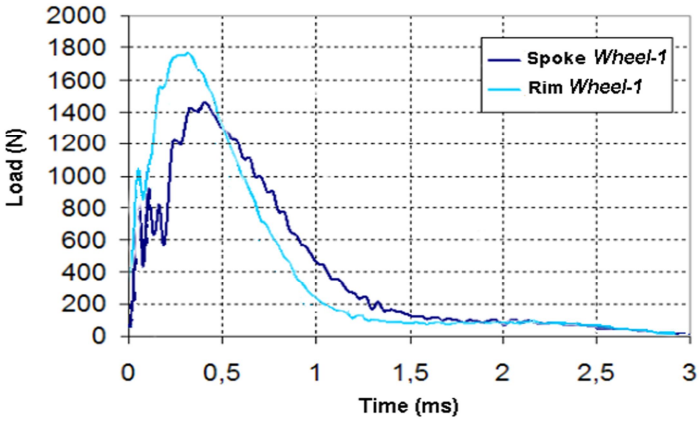

(a)

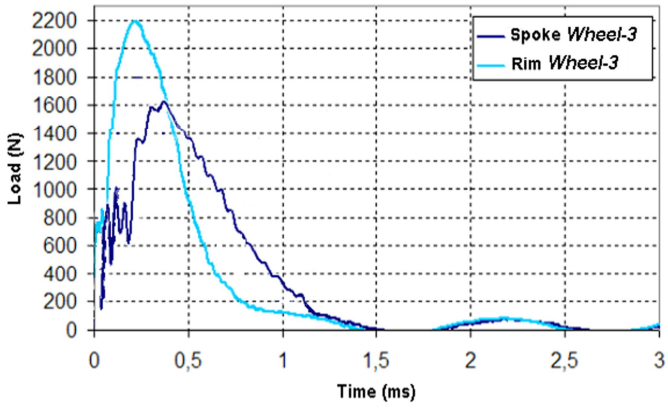

(b)

Fig. 7. Load-time curves of samples obtained from spoke and rim area of (a) wheel-1 and (b) wheel-3.

From both figures 7a and 7b, it is possible to observe that the samples drawn from the spoke zone show lower F_m values, but higher time to fracture (T) and time at the peak load (T_m). Vedani and Mapelli (2001) showed that the crack growth stability increases if the ratio between propagation energy and nucleation energy increases and the load reduction becomes slower.

Total absorbed energy was split into the two main complementary contributions, W_m and W_p, measured as previously described and reported as a percentage of the total impact energy. In figure 8 it is possible to observe that W_p values are in a range of 60-75% and the highest values are shown by the specimens drawn from as cast wheel-1, which shows thereby the lowest energies at maximum load. W_p values are generally higher in the region of spoke where the standard deviation is also higher.

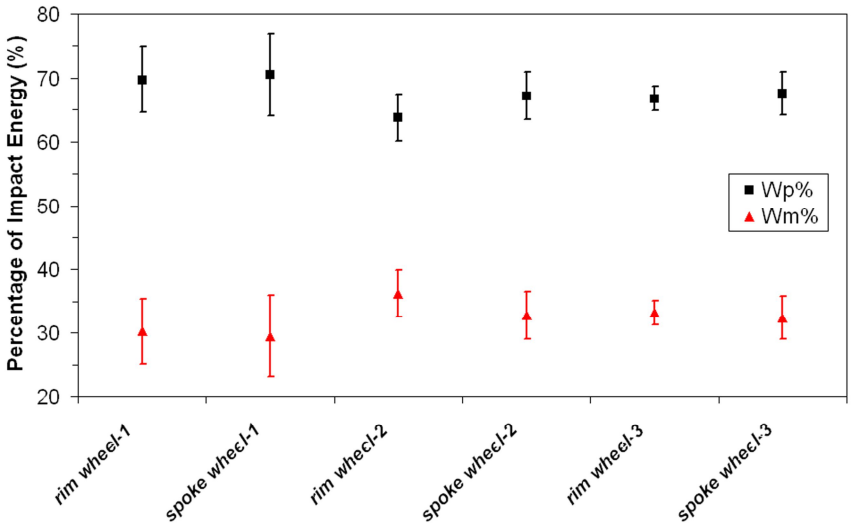

Fig. 8. Percentage of energy absorbed during crack nucleation and propagation and measured at different positions of the wheels analysed. The standard deviations are shown as error bars.

Considering the position of samples, it is necessary to note that the spokes are generally thicker (~15 mm) than the rim (~10 mm), which is the first zone to solidify, while the spoke and the hub zones are the last

ones. Therefore, the microstructure in the rim region is finer, with higher mechanical properties. This is confirmed by higher F_m values in the zone of the rim. Increasing the maximum load, the load-time curves shifts towards shorter times to fracture with lower percentage of propagation energy. The samples taken from the spokes show W_p values higher than the ones drawn from the rim.

The ductility of the material depends on the hardening treatment and also on the size and the morphology of silicon particles. The highest ductility of the specimens drawn from as cast wheel-1 can be attributed to the lower amount of hardening precipitates, leading to a reduction in stresses. The strontium modification is likely to have modified the size and the shape of the silicon particles, increasing the volume fraction of the plastic aluminium matrix.

While in wheels-2 and -3 the modification of the cast alloy with strontium and the solution treatment changed the silicon particles size and morphology, the highest density of β'-Mg_2Si precipitates with their needle-like shapes and brittle behaviour, increased the micro stresses; as showed by Zhang et al. (2002), this resulted in the reduction of α-Al matrix deformation, thus decreasing ductility. These precipitates are brittle and may fracture at very low strains during deformation, accelerating the growth of the crack. Blackmun (1968) argued that casting defects have a deleterious effect on mechanical properties and their distribution could not be uniform throughout the whole casting, consequently creating a non-uniform distribution of mechanical properties. This could explain the different scattering level in impact properties observed in the Charpy specimens drawn from the same wheel.

3.2.1. Relationship between impact properties and SDAS

In table 2, SDAS and impact energy values for the wheels analysed are reported. Due to the same geometry of the hub, SDAS values were

similar in this region. While wheel-1 showed the lowest SDAS values in the spoke and rim regions, a coarser microstructure appeared in wheels-2 and -3. This behaviour can be explained considering the different weight and mass distribution of wheel-1. The increased number of spokes and a wider rim made possible to reduce the spoke and rim thickness, obtaining a finer microstructure. The slight difference of geometry and weight between wheel-2 and -3 didn't evidence a significant change in the scale of microstructure.

SDAS measurements were correlated to the impact energy values with the aim to investigate the microstructural effect on impact properties. In accordance with Li et al. (2004), it was possible to understand from table 2, there exists an inverse correlation between SDAS and impact energy, a finer microstructure corresponds to an higher impact energy.

Table 2. SDAS and impact energy values in the wheels analysed. Average values and standard deviation are given.

Location	Wheel-1		Wheel-2		Wheel-3	
	SDAS (μm)	Impact Energy (J)	SDAS (μm)	Impact Energy (J)	SDAS (μm)	Impact Energy (J)
Hub	59±5	-	59±6	-	57±7	-
Spoke	35±5	1,53±0.11	42±7	2,24±0.20	39±4	2,75±0.32
Rim	23±7	1,55±0.10	28±4	2,55±0.22	26±4	2,41±0.29

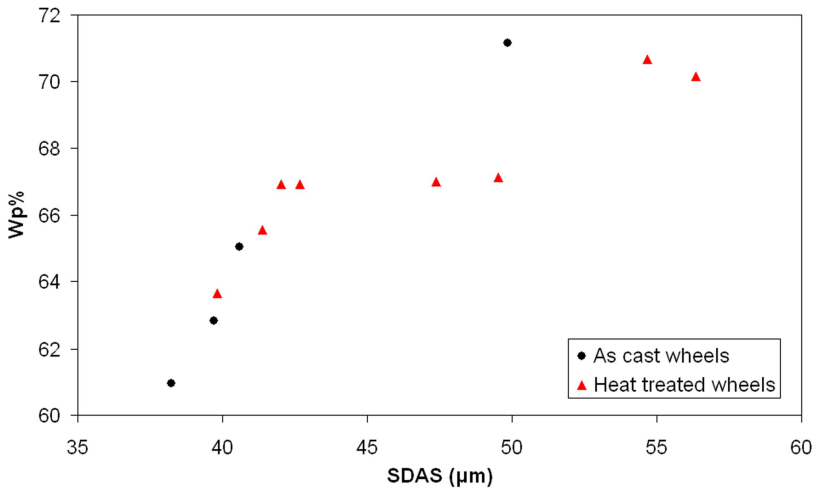

Fig. 9. Correlation between SDAS and W_p% (percentage of energy absorbed during crack propagation).

In figure 9, the crack propagation energy (W_p) has been correlated to SDAS values for the as cast and the T6 heat treated wheels. A direct correlation has been found, not depending on the wheel's temper.

3.2.2. Microstructural analysis of fracture profiles

The crack crosses the interdendritic eutectic region, where a significant fraction of cracked eutectic silicon and intermetallic particles is found, following the dendritic profile of the α-Al solid solution. In figures 10a-c the fracture profiles of samples taken from the different wheels can be seen. In agreement with Berto et al. (2004), who developed an analytical solution for the stress field around a V-notch, secondary cracks, parallel to the principal crack and normal to the tensile stress induced by the presence of the V-notch, can be observed. The crack path follows regions where there are hard and brittle eutectic silicon and intermetallic particles.

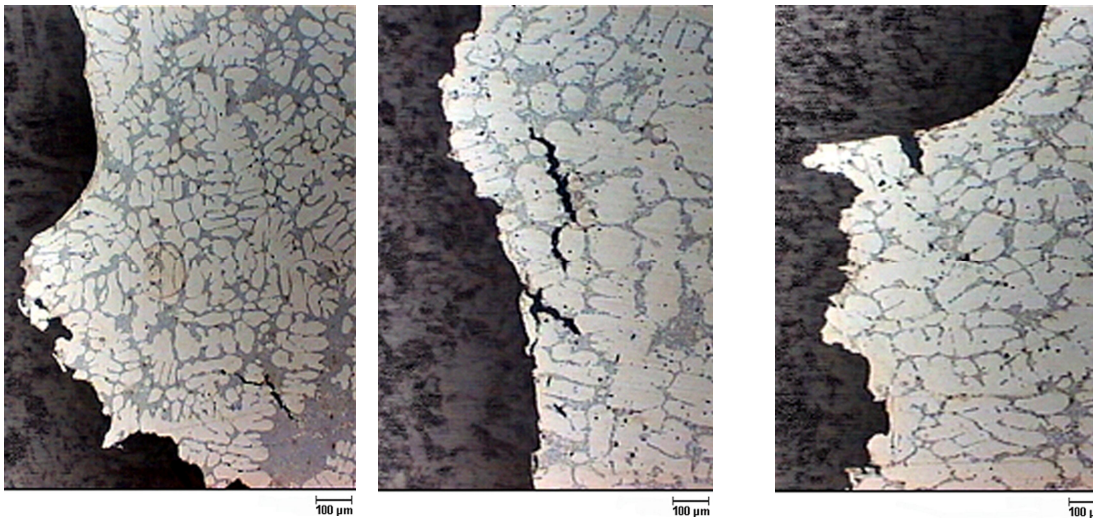

(a) (b) (c)

Fig. 10. Optical micrographs of the fracture profiles of samples drawn from (a) the rim of wheel-1 and from (b) the spoke of wheel-2 and (c) wheel-3. Secondary cracks are evident.

3.2.3. SEM analysis of fracture surfaces

As it can be seen in figure 11a and according to Warmuzek (2004), the SEM analysis of the fracture surface of a sample taken from the spoke of wheel-2 reveals a transcrystalline fracture of medium-developed surface; regions of cleavage facets are visible in the silicon precipitates and brittle intermetallic phases. In figure 11b the fracture surface of a sample drawn from the rim of wheel-1 reveals the presense of shrinkage porosity and the interdendritic path of the crack, that is the fracture profile follows the interdendritic eutectic zone. The edges of the deformed and fractured micronecks in α-Al solid solution with visible traces of microdeformation (dimples) are shown in figure 11c.

Fractures in the two-phase region were found, as put in evidence in figure 11d where the early stages of decohesion are visible on the interface between α-Al and silicon. In the microregion of the α-Al solid solution, the dimples have been formed around the cracked silicon particles as a result of plastic deformation of the matrix.

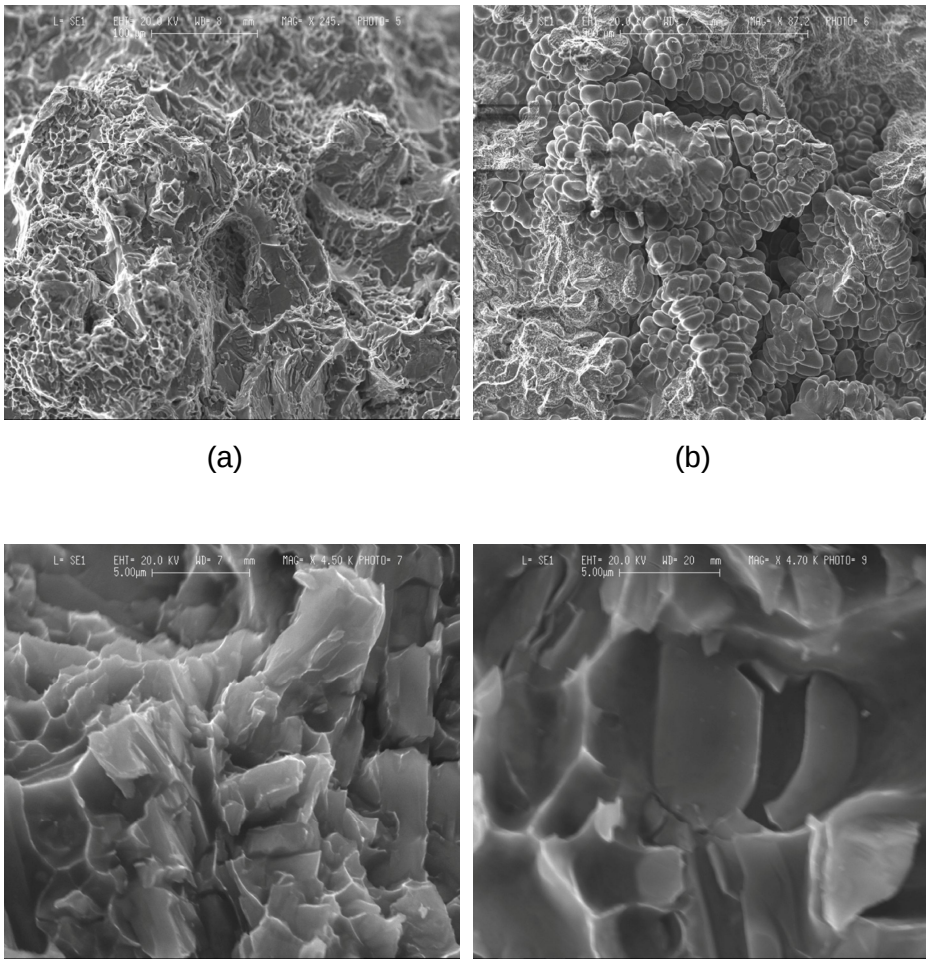

(a) (b)

(c) (d)

Fig. 11. Features of the fracture surfaces of the Charpy specimens drawn from the wheels analysed as revealed by SEM. (a) Transcrystalline and ductile fracture from the spoke of wheel-2; (b) interdendritic fracture from the rim of wheel-1; (c) micronecks and dimples from the rim of wheel-1; (d) cleavage fracture in the silicon precipitate from the rim of wheel-3.

The presence of secondary phases were revealed on the fracture surfaces of the samples analysed. An example is shown in figure 12 for a sample drawn from the spoke of wheel-3. The EDS analysis indicated the nature of the precipitate as brittle β-AlFeSi platelets (figure 12).

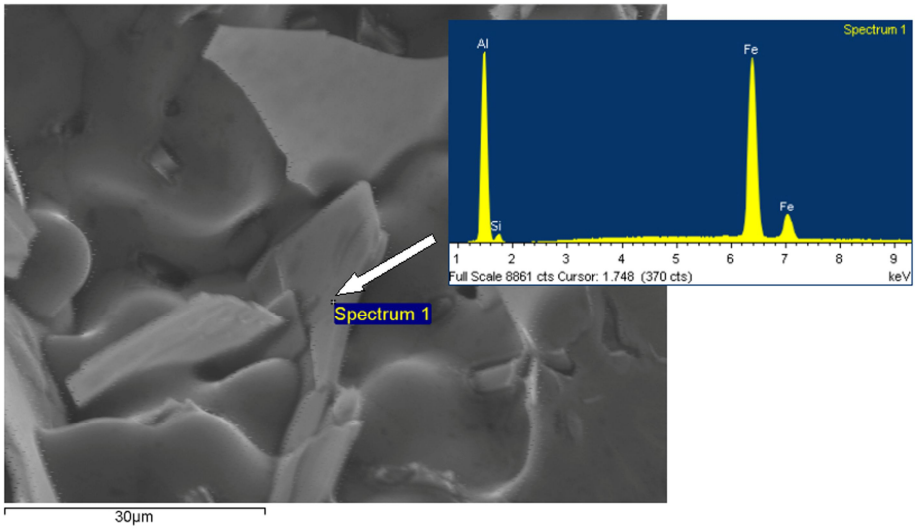

Fig. 12. SEM micrograph of ß-AlFeSi platelet, on the fracture surface of sample drawn from the spoke of wheel-3, with EDS spectra.

3.3. Porosity measurement

The preliminary X-ray analysis, carried out on each wheel, revealed the presence of macro porosity both in the spokes and in the rim. The qualitative results obtained with the X-ray equipment were quantitative confirmed by density measurements of Charpy samples drawn from wheels-2 and -3. Figure 13 shows the percentage porosity of wheels-2 and -3 in different positions and the standard deviations as error bars. Wheel-3 presents the highest porosity content, mainly concentrated in the zone of the spoke, while the percentage porosity in wheel-2 appears lower, revealing good casting quality. The elevated standard deviation demonstrates a non-homogeneous distribution of porosity inside the casting and consequently inside the Charpy specimens.

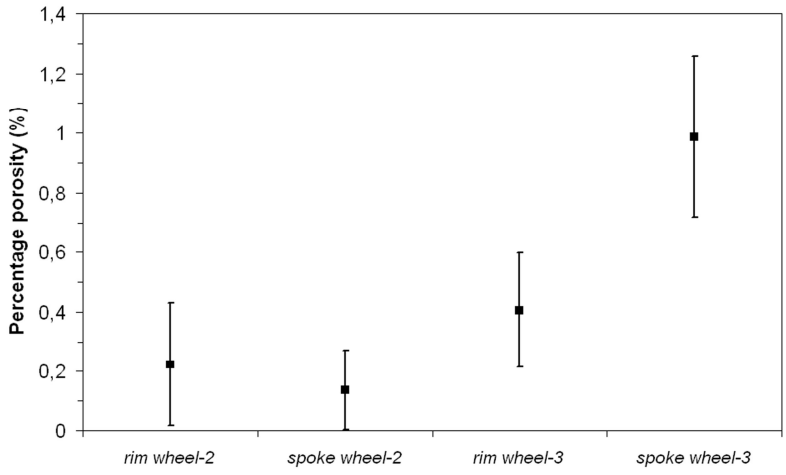

Fig. 13. Percentage porosity measured at different positions of the wheels analysed. The standard deviations are shown as error bars.

In order to individuate the macro porosity distribution, the Charpy samples were mapped with micro focus X-ray equipment. While in some samples the presence of defects extends throughout the specimen, involving also the zone around the notch (figure 14), other samples did not show defects close to the V-notch.

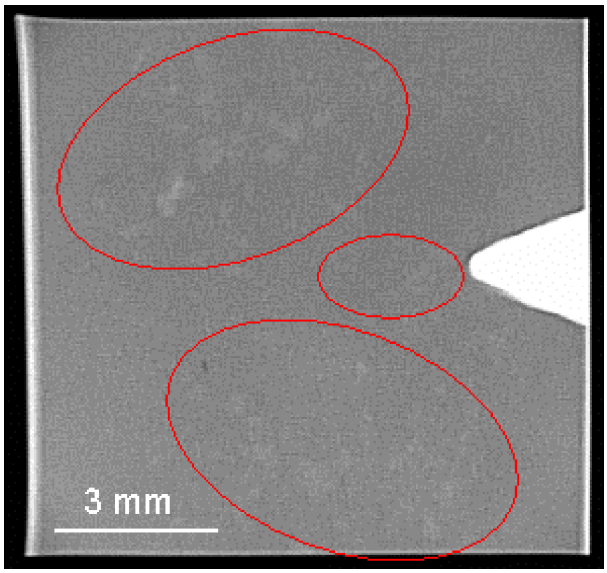

Fig. 14. Micro focus X-ray image of Charpy sample showing the presence of porosity around the notch.

To demonstrate the influence of defects' distribution on impact properties, the impact energy of some samples, drawn from the spoke of wheel-3, is sorted in figure 15, where some representative X-ray images, taken in the zone around the V-notch, are also shown. The X-ray images refer to a high (a), medium (b) and low (c) defect content. This is to demonstrate how the distribution of defects is not uniform in the region of the spoke of wheel-3, consequently creating a non-uniform distribution of impact properties, and how casting defects become critical when concentrated around the notch where they reduce the load bearing area of Charpy specimens. Therefore, the presence of porosity is critical on impact properties and can overcome the effect of the microstructure.

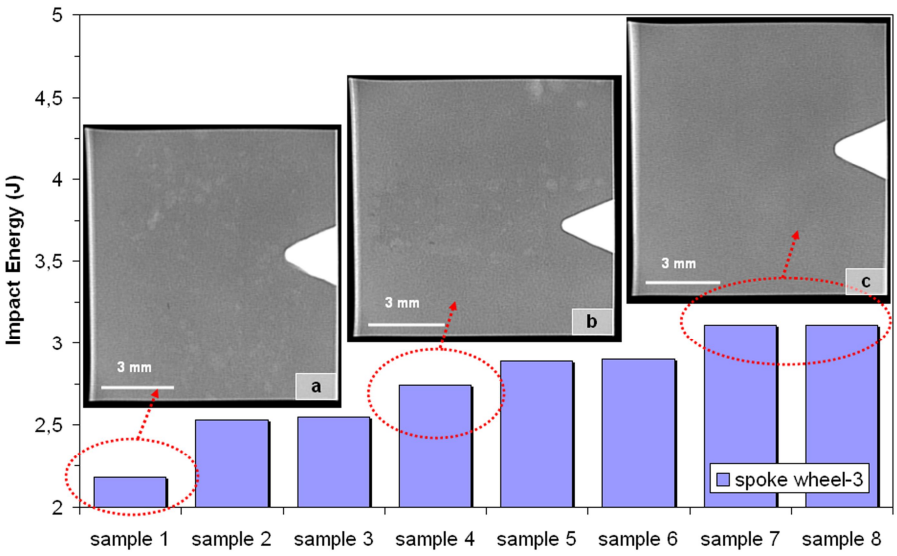

Fig. 15. Impact energy of some samples drawn from the spoke of wheel-3 associated with respective X-ray images, taken in the zone around the V-notch. The X-ray images refer to a high (a), medium (b) and low (c) defect content.

3.4. Computer simulation results

Campbell (2003) demonstrated that an important requirement for good casting quality of an aluminium wheel is optimal die filling, avoiding turbulence of the melt. Figure 16 shows the melt velocity at 20% and 70% of die filling of 7-spoke wheel-1. The results are displayed for half the casting. At the start of die filling the flow speeds increase with an increase in the build-up pressure, increasing the risk of turbulence. Earlier Kuo et al. (2001) and later Schroth and Schemme (2003) showed that a flow speed higher than 0.5 m/s results in breaking up of the melt front, leading to oxidation of the melt, inclusion of oxide films and air entrapment throughout a low pressure die cast wheel. As previously seen, impact properties are strongly influenced by the presence of defects. An important feature is the different magnitude of the high melt speed and the point of time of its occurrence. With the reduction of the feed cross-section in the relatively thin spokes the melt locally accelerates in this region (Figure 16a), with a maximum melt velocity of 0.27 m/s. On reaching the larger volume with entry into the rim, the speed of the melt reduces until the wheel is completely filled (Figure 16b). The maximum melt velocity is about 0.04 m/s in the region of rim. From numerical simulation results it was possible to demonstrate how a good compromise between laminar filling and decreasing melt temperature was obtained. Bonollo et al. (1999) demonstrated that too slow die filling increases the risk of freezing by decreasing the melt temperature below the alloy-dependent coherence temperature. Numerical calculations showed a melt temperature higher than 617°C during the filling and no evidence of solidification cavities caused by a premature freezing of the melt. The 5-spoke wheels-2 and -3, even with a different geometry, reflect similar filling behaviour of wheel-1, i.e. a mean melt velocity lower than 0.3 m/s.

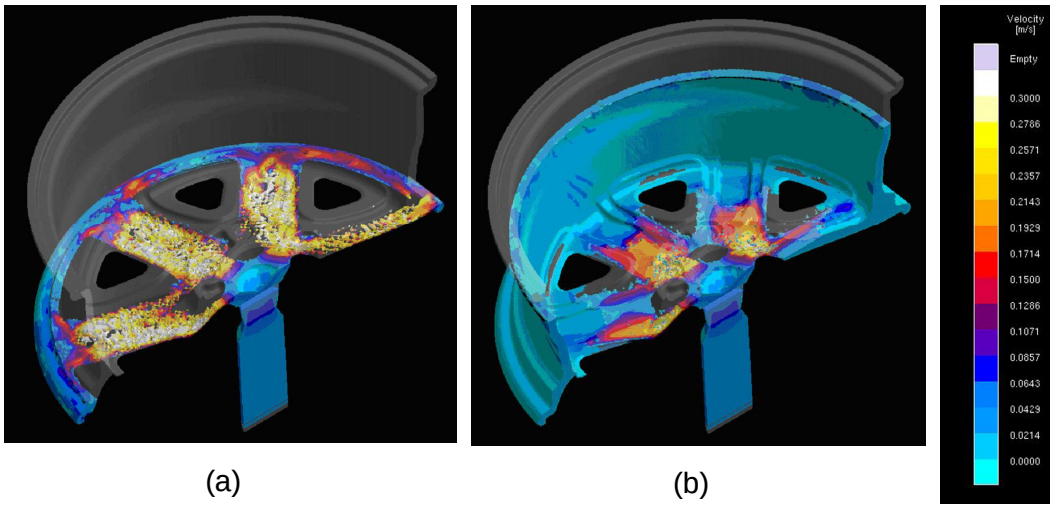

Fig. 16. Calculated melt velocity at (a) 20% and (b) 70% of die filling of wheel-1.

After completion of die filling the wheel starts to solidify. Figure 17 presents calculated solidification times, from numerical simulation, with the corresponding microstructure within wheel-2. In accordance to Kurz and Fisher (1998), solidification times were also estimated by means of SDAS measurements. A comparison between calculated and estimated solidification times was carried out (Figure 17). As it is possible to observe the relationship is good, testifying the ability of numerical simulation codes to predict the local solidification conditions and the characteristics of casting components. Wheels-1 and -3, even with different geometries, reflect similar solidification behaviour, as previously evidenced by SDAS measurements.

Ideally, solidification should occur directionally, starting from the rim, via the spokes to the hub. Simulation of casting solidification revealed problem areas in the junction zone between the spoke and the rim within wheel-2, specifically, a hot spot caused by increased thickness. Longer solidification time in this zone is opposed to that of the spoke and the rim. Therefore, the hot spot in the junction zone between the spoke and the rim is a critical region for feeding. The casting shrinkage is indicated by a feeding criterion in figure 18, where, in addition to the

shrinkage porosity in the junction zone between the spoke and the rim, smaller solidification cavities are present in the rim area. The presence of defects was confirmed by means of X-ray inspections and metallographic analysis (Figure 18).

The feeding criterion was applied to wheels-1 and -3 and revealed an higher content of shrinkage porosity in the rim zone and in the junction zone between the spoke and the rim. This could confirm the highest porosity amount from the density measurements of Charpy samples taken from wheel-3 even if, as previously said, the presence of defects is critical when concentrated around the notch.

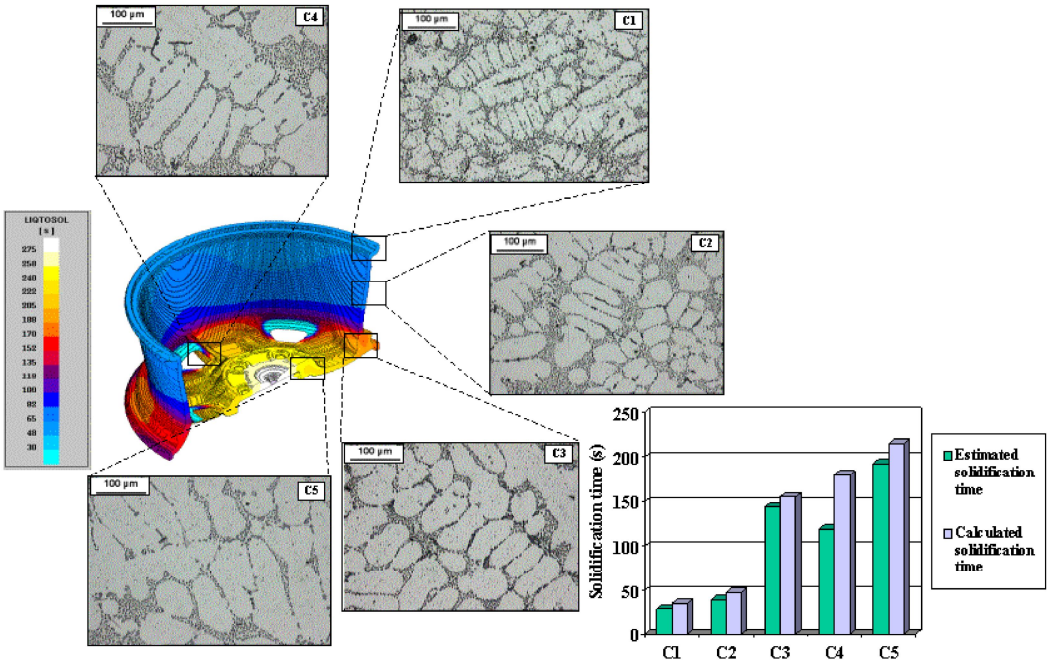

Fig. 17. Calculated solidification times with corresponding microstructure within wheel-2. Solidification times, estimated by means of SDAS measurements and calculated with a numerical simulation approach, were compared.

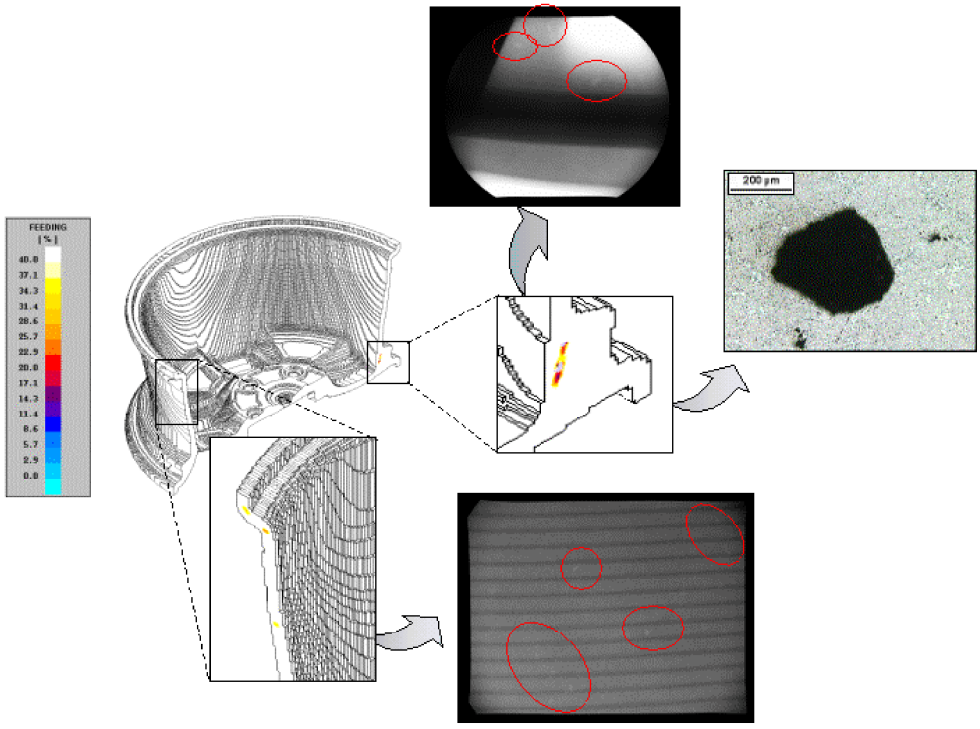

Fig. 18. Shrinkage porosity in the rim area and in the junction between the spoke and the rim within wheel-2. These zones are critical for feeding. The casting shrinkage is indicated by a feeding criterion.

4. CONCLUSIONS

Impact strength tests have been performed on Charpy V-notch specimens drawn from three different A356 17-inch wheels, produced by low pressure die casting. While one wheel is a 7-spoke wheel in the as cast temper, the other two wheels, which are 5-spoke wheels in the same T6 condition, differ on the geometry and thickness of spokes and rims.

Based on the results obtained regarding the influence of microstructure on impact properties, the following conclusions can be drawn:

- Impact energy values are lower in the as cast microstructure than in the T6 heat treated one.

- A finer microstructure always corresponds to higher impact strength.
- The resistance to crack propagation values (W_p) are in the range of 60-75% of the total absorbed energy and the highest values are shown by the as cast microstructure.
- A direct correlation between W_p and SDAS is found.
- The crack crosses the interdendritic eutectic region where the microstructural analysis has revealed microshrinkage porosity, cracked eutectic silicon with different size and morphology in the as cast and in the T6 heat treated wheels, the presence of cracked intermetallic particles.

Based on the results obtained regarding the influence of defects on impact properties, the following can be summarised:

- The preliminary X-ray analysis, carried out on each wheel, has revealed the presence of porosity both in the spokes and in the rim. The qualitative results obtained with the X-ray equipment are quantitative confirmed by density measurements of Charpy samples. The elevated standard deviation of density measurements demonstrates a non-homogeneous distribution of porosity inside the casting and consequently inside the Charpy specimens.
- Casting defects become critical when concentrated around the V-notch where they reduce the load bearing area of Charpy specimens. Therefore, the presence of defects is critical on impact properties and can overcome the effect of the microstructure.

In terms of utility, numerical simulation has been demonstrated to be able to predict the formation of macro-defects, as indicated by a feeding criterion, and the final scale of microstructure within the casting. From these results, numerical simulation has confirmed its potential as an engineering tool to predict the impact properties throughout the casting.

ACKNOWLEDGEMENTS

The Authors acknowledge for the experimental contribution to this research dr. E. Capatti, dr. F. Piasentini, dr. F. Massari and dr. N. Tomanin. Many thanks are also due to dr. E. Della Rovere and G. Mazzacavallo. Many thanks are also due to dr. N. Gramegna for helping with MAGMASOFT® simulations.

REFERENCES

1. Berto, F., Lazzarin, P., Wang, C.H., 2004. Three-dimensional linear elastic distributions of stress and strain energy density ahead of V-shaped notches in plates of arbitrary thickness. Int. J. Fract. 127, 265-282.

2. Blackmun, E.V., 1968. Casting. In: Kent, R., Van Horn, Aluminum vol. III – Fabrication and Finishing, third ed., American Society for Metals, Metals Park, OH, pp. 43-80.

3. Bonollo, F., Gramegna, N., Odorizzi, S., 1999. La pressocolata delle leghe di alluminio: simulazione numerica del processo, first ed., Edimet, Brescia.

4. Brown, R., 1999. Foseco non-Ferrous foundryman's handbook, eleventh ed., Butterworth-Heinemann, Oxford.

5. Cáceres, C.H., Davidson, C.J., Griffiths, J.R., 1995. The deformation and fracture behaviour of an Al-Si-Mg casting alloy. Mater. Sci. Eng. A 197, 171-179.

6. Cáceres, C.H., Selling, B.I., 1996. Casting defects and the tensile properties of an Al-Si-Mg alloy. Mater. Sci. Eng. A 220, 109-116.

7. Campbell, J., 2003. Castings, second ed., Elsevier Butterworth-Heinemann, Oxford.

8. Flinn, R.A., 1963. Fundamentals of metal casting, first ed., Addison-Wesley Publishing Company, Massachusetts.

9. Kuo, J.-H., Hsu, F.-L., Hwang, W.-S., 2001. Development of an interactive simulation system for the determination of the pressure-time relationship during the filling in a low pressure casting process. Sci. Technol. Adv. Mater. 2, 131-145.

10. Kurz, W., Fisher, D.J., 1998. Fundamentals of solidification, fourth ed., Trans. Tech. Publications, Switzerland.

11. Li, Z., Samuel, A.M., Samuel, F.H., Ravindran, C., Doty, H.W., Valtierra, S., 2004. Parameters controlling the performance of AA319-type alloys Part II. Impact properties and fractography. Mater. Sci. Eng. A 367, 111-122.

12. MAGMASOFT® v.4.2, 2002. MAGMAlpdc Module Manual, MAGMA Giessereitechnologie GmbH.

13. Murali, S., Raman, K.S., Murthy, K.S.S., 1992. Effect of magnesium, iron (impurity) and solidification rates on the fracture toughness of Al-7Si-0.3Mg casting alloy. Mater. Sci. Eng. A 151, 1-10.

14. Paray, F., Kulunk, B., Gruzleski, J.E., 2000. Impact properties of Al-Si foundry alloys. Int. J. Cast Met. Res. 13, 17-37.

15. Pedersen, L., 1999. Solution heat treatment of AlSiMg foundry alloys, PhD thesis, Norwegian University of Science and Technology (NTNU), Trondheim.

16. Schroth, A., Schemme, D., 2003. Simulation in modern quality management systems – Simulation assists the implementation of quality management systems in foundries. Casting Plant and Technology 19, 8-18.

17. Shivkumar, S., Wang, L., Keller, C., 1994. Impact properties of A356-T6 alloys. J. Mater. Eng. Perform. 3, 83-90.

18. Sicha, W.E., 1971. Properties of commercial casting alloys. In: Kent, R., Van Horn, Aluminum vol. I – Properties, Physical Metallurgy and Phase Diagram, fourth ed., American Society for Metals, Metals Park, OH, pp. 277-302.

19. Srivastava, M.C., Lohne, O., Arnberg, L., Laukli, H.I., Gjestland, H., 2006. Energy absorption of HPDC aluminium and magnesium alloys. In: Proc. High Tech Die Casting 2006, Vicenza, Italy, paper 10.

20. Street, A.C., 1986. The diecasting book, second ed., Portcullis Press, London.

21. Vedani, M., Mapelli, C., 2001. Effect of thermal treatments on microstructure and impact toughness of die-cast Mg-Al-Mn alloys. Mat. Sci. Tech. 17, 938-944.

22. Wang, Q.G., Cáceres, C.H., 1998. The fracture mode in Al-Si-Mg casting alloys. Mater. Sci. Eng. A 241, 72-82.

23. Warmuzek, M., 2004. Aluminium-Silicon Casting Alloys: Atlas of Microfractographs, first ed., ASM International.

24. Zhang, D.L., Zheng, L.H., StJohn, D.H., 2002. Effect of a short solution treatment time on microstructure and mechanical properties of modified Al-7wt.%Si-0.3wt.%Mg alloy. J. Light Met. 2, 27-36.

Article 2

EFFECT OF EUTECTIC MODIFICATION AND THE SOLIDIFICATION RATE ON THE IMPACT STRENGTH OF A356 ALUMINUM-SILICON ALLOYS

Mattia Merlin*, Lorenzo Pivetti**, Gian Luca Garagnani*

* Department of Engineering - ENDIF
University of Ferrara
I-44100 Ferrara
Italy

** Fonderia Scacchetti Leghe Leggere S.r.l.
I-41038 San Felice sul Panaro (MO)
Italy

Metallurgical Science and Technology, 2008, **26-1**, 22-29

ABSTRACT

The impact energies of A356 aluminum-silicon alloys have been measured using a Charpy impact tester. The Charpy specimens have been machined from cast plates with the same geometry and produced in sand moulds. Unmodified, sodium-modified and strontium-modified castings have been tested. In this paper, the effects of eutectic modification and of the cooling rate on the impact properties of A356 aluminum-silicon alloys have been studied. When the value of the cooling rate is the same, unmodified samples show lower impact energies than modified ones: the effect of eutectic modification is emphasized in strontium-modified samples. Moreover, a finer microstructure always corresponds to higher impact strength and an inverse correlation between impact energy and secondary dendrite arm spacing (SDAS) has been found. The fracture profile and surface of cracked samples have been analyzed by means of Optical and Scanning Electron Microscopes, in order to investigate the effect of eutectic silicon and intermetallic particles. Numerical simulations have been carried out to study the filling and the solidification behavior of the sand cast plates under different cooling conditions, in order to predict the final microstructure and shrinkage formation. A good correspondence between SDAS values, calculated by means of numerical simulations and measured with the linear intercept method, has been found.

KEYWORDS

Sand A356 castings, impact properties, modification, microstructure, numerical simulation.

1. INTRODUCTION

Foundry processes have shown a great degree of technological innovation in recent years. Aluminum-silicon alloys are the most important and widely used casting alloys, due to excellent castability and a good compromise between mechanical properties and lightness, and they are commonly used in a variety of engineering applications for producing parts with complex shapes. In literature several authors have analyzed the relationship between mechanical properties and the microstructure of aluminum-silicon alloys with the aim of developing a final product with good mechanical properties. It can be seen that the impact test is a useful method in evaluating the effects of process parameters and microstructures on the dynamic fracture toughness of engineering materials. Apelian et al. demonstrated that the mechanical properties of Al-Si-Mg castings are controlled by secondary dendrite arm spacing (SDAS) and the silicon particles morphology [1].

Impact tests can provide a useful estimation of the ductility of an alloy under conditions of rapid loading. Moreover, Li et al. analyzed the effect of various alloying elements and different heat treatments on A319-type alloys by means of an instrumented impact test [2]. An increase in the magnesium content determines a drop in the absorbed energy and a similar behavior can be observed when increasing the iron content; in particular iron is deleterious because of the precipitation of β-Al_5FeSi platelets. When investigating the impact behavior of four different aluminum-silicon alloys, in terms of total absorbed fracture energy and crack initiation and propagation energies, Paray et al. considered the effect of strontium additions and of different solidification rates on microstructures [3]. In cast aluminum alloys both yield strength and ductility are improved by the T6 treatment, due to the precipitation of fine β'-Mg_2Si particles and the spheroidization of the eutectic silicon particles [4]. Other authors, by means of Charpy impact tests performed on sand mould castings, have

analyzed the effect of strontium modification in reducing the solution treatment time [5].

The aim of this research is to measure the impact energy of A356 aluminum-silicon alloys by means of instrumented Charpy impact tests. Specimens have been drawn from plate castings produced in sand moulds and have been subjected to T6 treatment. The effect of eutectic modification and of different cooling rates on microstructures have been taken into account. Impact properties, such as total absorbed energy, maximum load, crack nucleation and propagation energies, have been correlated to the microstructures. Preliminary X-ray investigations have been carried out on all machined samples to verify the absence of macroscopic porosity and defects near the V-notch, which affect the impact test results. Microstructural analyses have been performed on fractured samples by means of Optical Microscopes (OM) and Scanning Electron Microscopes (SEM) with Energy Dispersive X-ray (EDS) microprobes, with the aim of determining SDAS, the presence of porosity and secondary phases, and of analyzing the fracture profile and surface. The sand casting process of the plate castings has been studied preliminarily, using numerical simulations and the results have been compared with those obtained by microscopy.

2. EXPERIMENTAL PROCEDURE

Research has been performed on plates produced by the sand mould casting process. Instrumented impact tests have been carried out on KV Charpy specimens machined from six A356 plate castings. In order to evaluate the effect of the solidification rate and of the eutectic modification on impact strength, three different alloy compositions and two different cooling rates have been investigated.

2.1. Alloy and casting system

The plate castings were produced using the hypoeutectic A356 in three conditions: unmodified, sodium-modified and strontium-modified, as reported in Table 1.

Table 1. Alloy chemical compositions of A356.

Condition	Composition [wt%]						
	Si	Fe	Mg	Ti	Na	Sr	Al
unmodified	6.96	0.130	0.334	0.128	0.0004	<0.001	Bal.
sodium-modified	6.75	0.126	0.328	0.166	0.00836	0.002	Bal.
strontium-modified	7.03	0.131	0.323	0.168	0.0008	0.0208	Bal.

The metal was melted in an electric-induction furnace at 700 ± 5°C and the alloy was chemically analyzed by means of Optical Emission Spectroscopy (OES); unmodified, sodium-modified and strontium-modified plate castings were produced from the same melt. Before casting, the melt was degassed with nitrogen and Straube-Pfeiffer tests were performed to evaluate the molten quality.

Three plates were solidified in sand without any chills and three plates were solidified with the help of cast iron chills. The sand moulds were manufactured on the basis of a wood model; in Fig.1 a plate is depicted with a pouring system. In order to control the thermal history of the components, K-type thermocouples were inserted into the mould cavity and a Pico Technology® datalogger was used to monitor the cooling curves. After solidification, a T6 heat treatment was carried out on the plate castings; each plate was held at 525 ± 5°C for 8h, water quenched at 80°C and then artificially aged at 160 ± 5°C for 4h.

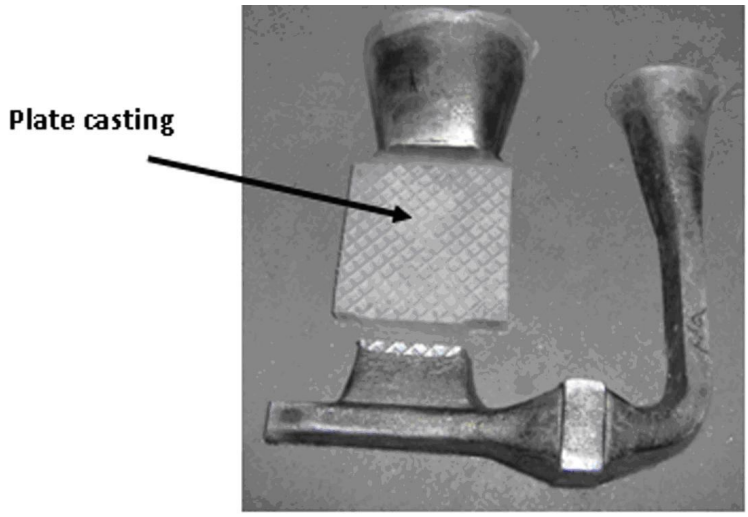

Fig. 1. Plate casting with pouring system.

2.2. Casting simulations

ProCAST software was used in order to numerically simulate the filling and the solidification of the plate castings with and without chills. The key-factor for the success of the simulation codes is the possibility of viewing the more critical regions of the casting. The CAD model of the casting was imported into ProCAST and the initial conditions for simulations were defined to reproduce the sand casting parameters. The results obtained from numerical simulations made it possible to verify the absence of macroscopic defects in the plate castings and to foresee filling velocity, porosity localization and SDAS (secondary dendrite arm spacing). This information is useful when choosing the drawing direction of the samples, in order to exalt the effect of microstructures on mechanical properties. The samples were drawn according to the longitudinal direction of the plate in both un-chilled and chilled castings.

2.3. X-ray investigation and impact testing

Charpy specimens 5 x 10 x 55 mm with a V-notch of 2 mm depth and a root radius of 0.25 mm were machined from the plate castings. In order to verify the absence of macroscopic defects, in particular around the notch, X-ray investigations were carried out on the samples.

Impact tests were performed using a 50 J Ceast instrumented pendulum; impact properties were measured according to UNI EN ISO 14556:2003. Total absorbed energy (W_t) was evaluated as the integral of the load-displacement curve throughout the test, the end of the test is assumed to be when the force reaches 2% of its peak. The crack initiation energy (W_m) and the propagation energy (W_p) were calculated: W_m is the energy at the maximum load (F_m), while W_p is the energy calculated from the maximum load at the end of the test.

2.4. Microstructural analysis and fractography

After impact testing, the samples were prepared for a metallographic inspection: Optical Microscopes and image analysis software were used in order to observe the fracture profile and to understand how the microstructure acts during the crack process. By means of the linear intercept method and considering ten random areas in each sample, SDAS average values were calculated.

SEM examination was also performed in order to study the fracture surfaces: the analysis of the main precipitates was carried out by means of Electron Dispersive Spectroscopy (EDS).

3. RESULTS AND DISCUSSION

3.1. Thermal analysis

Thermal analysis was implemented by means of K-type thermocouples with the aim of understanding the variations in microstructure in the sand plate castings, due to the absence or presence of cast iron chills. In each sand mould cavity, a thermocouple was used to record the cooling curves. By comparing Fig. 2 and Fig. 3, it is possible to note that solidification and cooling times are shorter in chilled castings than in un-chilled castings. Furthermore, in both figures the effect of modification is showed, in fact the strontium-modified and sodium-modified alloys have longer cooling times then the unmodified one. These variations in cooling time lead to differences in the microstructure, as described in section 3.2, and also affect the impact strength performance of the sand cast components.

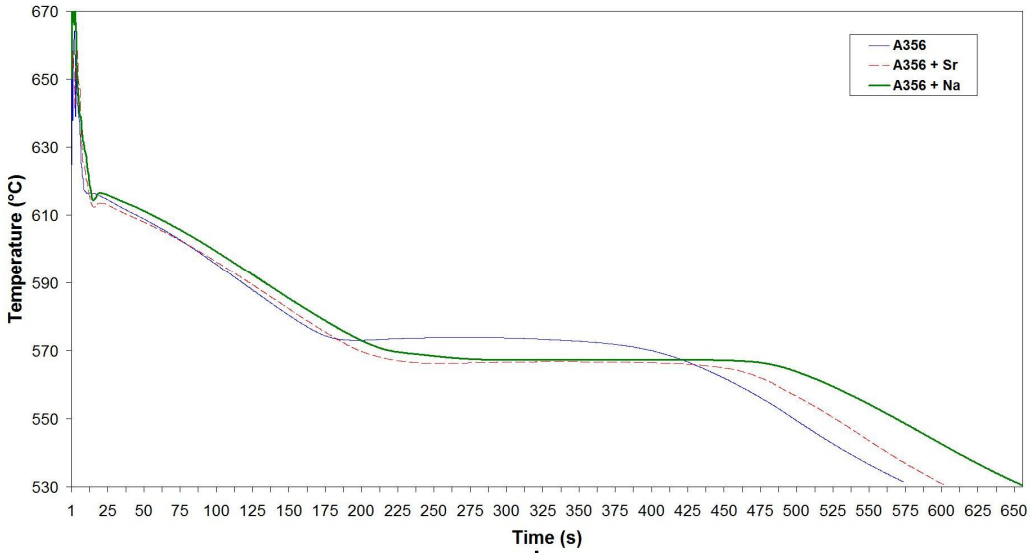

Fig. 2. Thermal history of the un-chilled sand plate castings.

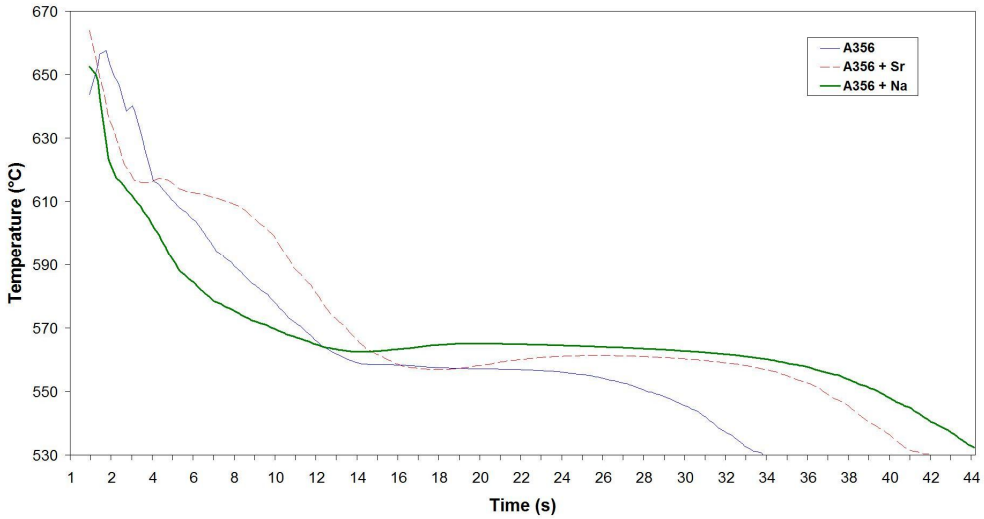

Fig. 3. Thermal history of the chilled sand plate castings.

3.2. Microstructural investigation

The typical microstructure of a sand cast A356 is characterized by the primary α-Al phase and the eutectic of aluminum and silicon. The microstructure coarseness is defined as the secondary dendrite arm spacing (SDAS), which is a function of the solidification time [6]; the higher the cooling rate, the finer the microstructure. The effect of modification with sodium or strontium, is the eutectic silicon microstructural change from acicular to fibrous. Fibrous, or better globular, eutectic silicon particles improve the impact properties of cast aluminum-silicon alloys [7]. The microstructures of the Charpy samples drawn from unmodified, sodium-modified and strontium-modified castings are reported in Figs. 4-6, respectively. The micrographs concerning the two different cooling rates are compared and it can be noted that the eutectic silicon distribution is less uniform in the sodium-modified samples than in the strontium-modified ones.

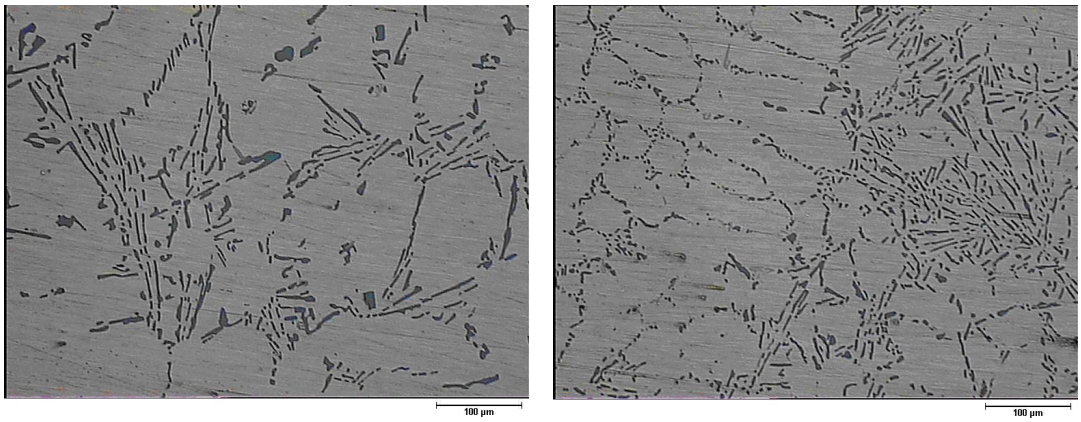

(a) (b)

Fig. 4. Microstructure of A356 unmodified alloy: a) un-chilled, b) chilled.

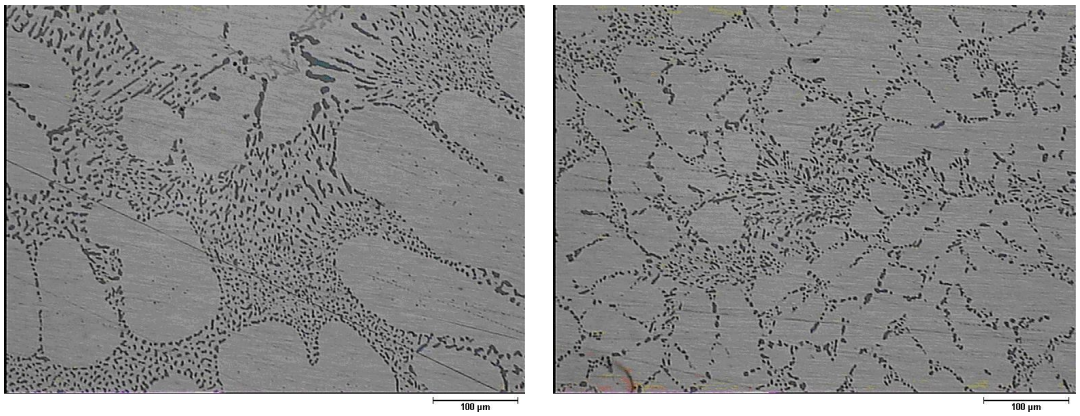

(a) (b)

Fig. 5. Microstructure A356 Na-modified alloy: a) un-chilled, b) chilled.

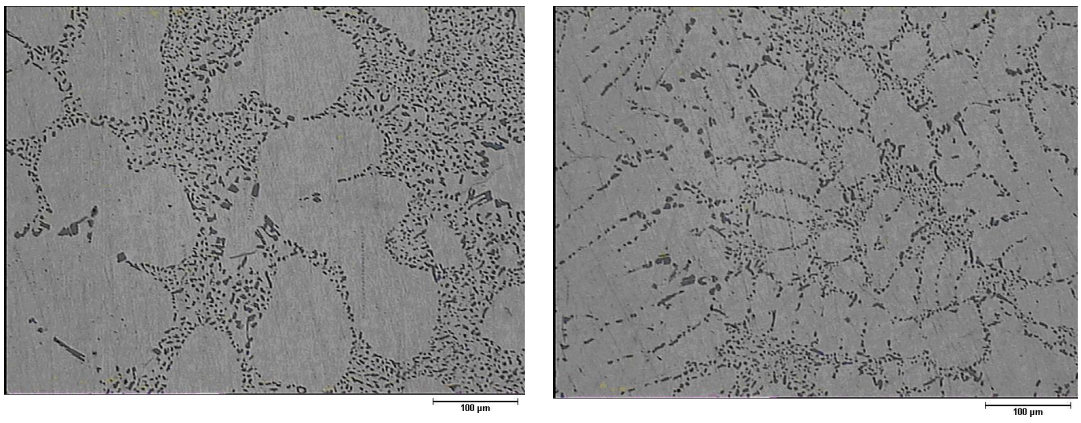

(a) (b)

Fig. 6. Microstructure A356 Sr-modified alloy: a) un-chilled, b) chilled.

Secondary phases, in particular Fe-rich intermetallics with the typical needle shape, have been observed in the samples. In Fig. 7 the $Al_{15}(Mn,Fe)_3Si_2$ phase, which has the morphology of the Chinese script, seems to coexist with the primary α-Al solid solution: even if Mn acts as a Fe-corrector promoting the formation of the Chinese script, needle-shaped β-phase can also be noted [6]. The presence of Fe in the alloy involves a loss in ductility, shock resistance and machinability [8]. Moreover, microshrinkage porosity has been observed, in particular an interdendritic cavity is reported in the micrograph in Fig.8.

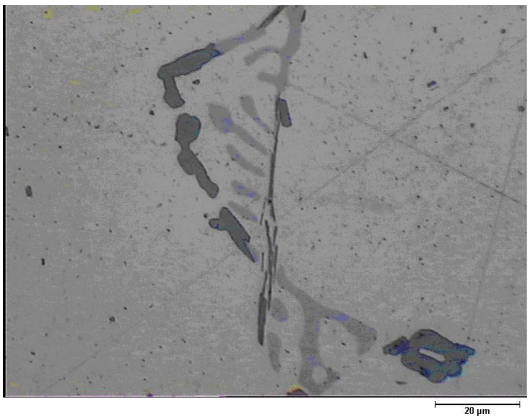

Fig. 7. Optical micrograph showing secondary phases particles.

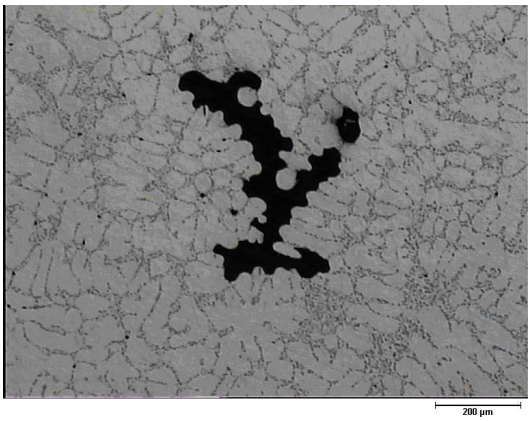

Fig. 8. Optical micrograph showing the presence of shrinkage porosity.

An analysis of the fracture profiles has been carried out in order to understand the impact strength results better. The micrograph in Fig. 9 shows that the main crack crosses the interdendritic eutectic region, following the dendritic profile of α-Al primary phase: secondary cracks can also be noted. In the eutectic region, brittle and hard eutectic silicon and intermetallic particles can be found, producing the typical step fracture. As can be seen in Fig. 10, several secondary cracks cross the eutectic brittle silicon particles.

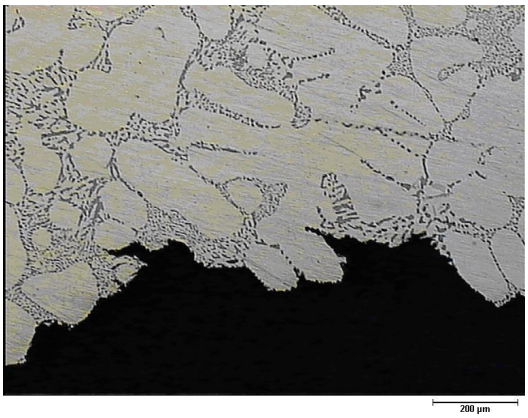

Fig. 9. Optical micrograph of the fracture profile of a sodium-modified sample.

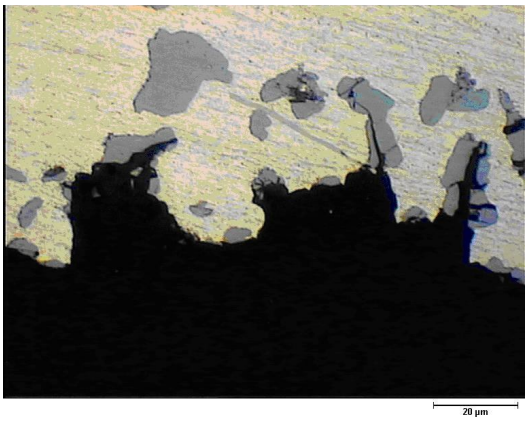

Fig. 10. Optical micrograph showing secondary cracks of eutectic silicon particles.

3.3. Impact strength

The average values of the total impact energy, obtained on the V-notch Charpy samples by using the instrumented impact testing method, and the deviations are reported in Fig. 11. The effects of the different cooling rates and of the alloy modification are evident.

The samples machined from the un-chilled castings show lower impact energies than the chilled ones. Notwithstanding, the maximum deviation in impact energy (~0,2J) of the un-chilled castings is lower with respect to the maximum deviation (~0,4J) of the chilled ones, as depicted in Fig. 11. The cast iron chills increase the impact strength values by about 140% in unmodified samples, while in modified ones the increase is at least 105%. It can also be noted that the modification of the alloy involves an increase in impact strength values, regardless of the cooling rate: the effect is emphasized in strontium-modified samples.

Concerning the maximum load values, the higher the cooling rate, the higher the peak force, as reported in Fig. 11; the peak force increases from 3854 N to 5516 N (about 43%) in the unmodified alloy. A similar trend is observed in the modified alloys.

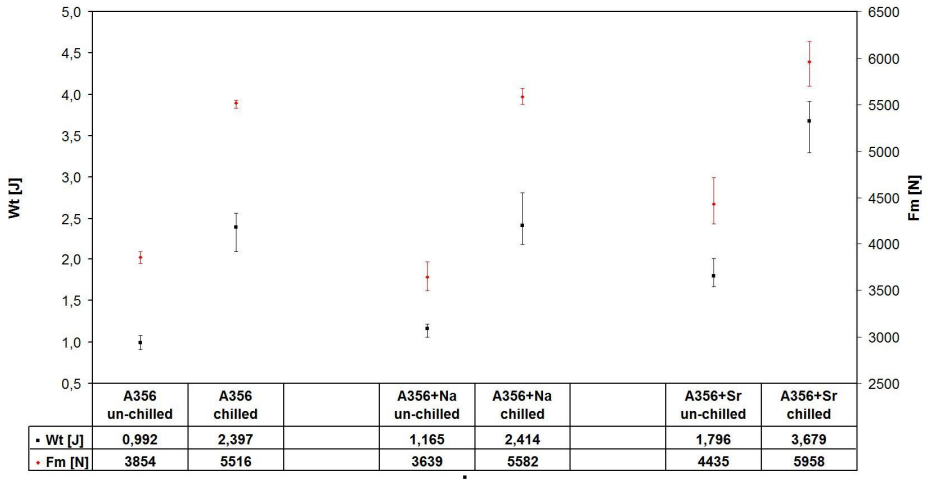

	A356 un-chilled	A356 chilled		A356+Na un-chilled	A356+Na chilled		A356+Sr un-chilled	A356+Sr chilled
▪ Wt [J]	0,992	2,397		1,165	2,414		1,796	3,679
▪ Fm [N]	3854	5516		3639	5582		4435	5958

Fig. 11. Impact energy and maximum load. Deviations from average values are shown as error bars.

Fig. 12 shows the load-displacement curves obtained from the instrumented impact testing machine. The curves refer to samples machined from the chilled plate castings and emphasize the effect of the modification on the peak force. The strontium-modified and sodium-modified samples show greater maximum loads than the unmodified one. Concerning modification, the strontium-modified sample shows the maximum value.

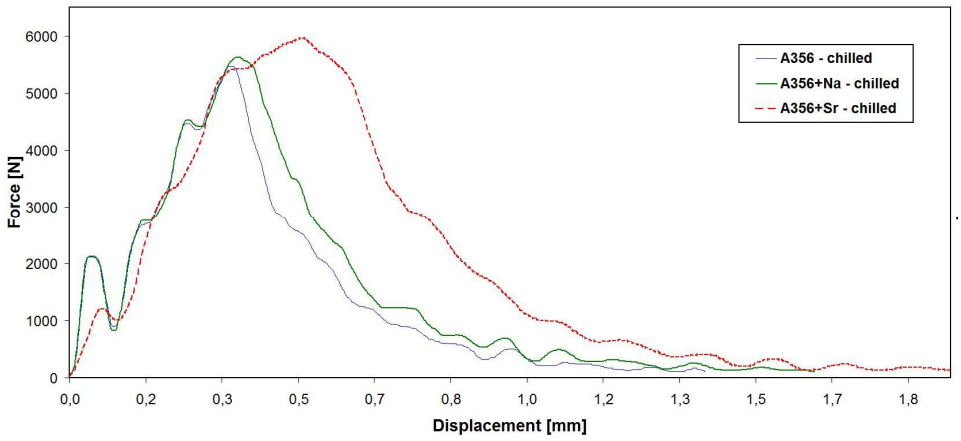

Fig. 12. Load-displacement curves for three samples machined from unmodified, Na-modified and Sr-modified chilled plate castings.

As explained above, the total impact energy has been split into the complementary contribution W_m and W_p. In Fig. 13 W_m and W_p are reported as percentages of the total absorbed energy and it can be noted that the W_p values are in the range 50-65%. In unmodified samples a great difference between chilled and un-chilled condition cannot be observed, deviations from the average values are high. On the contrary, in modified samples the increase in cooling rate corresponds to the decrease in W_p. The microstructure in the chilled samples is finer, with higher mechanical properties. This is confirmed by higher F_m values, but the propagation energy becomes lower when the maximum load is increased.

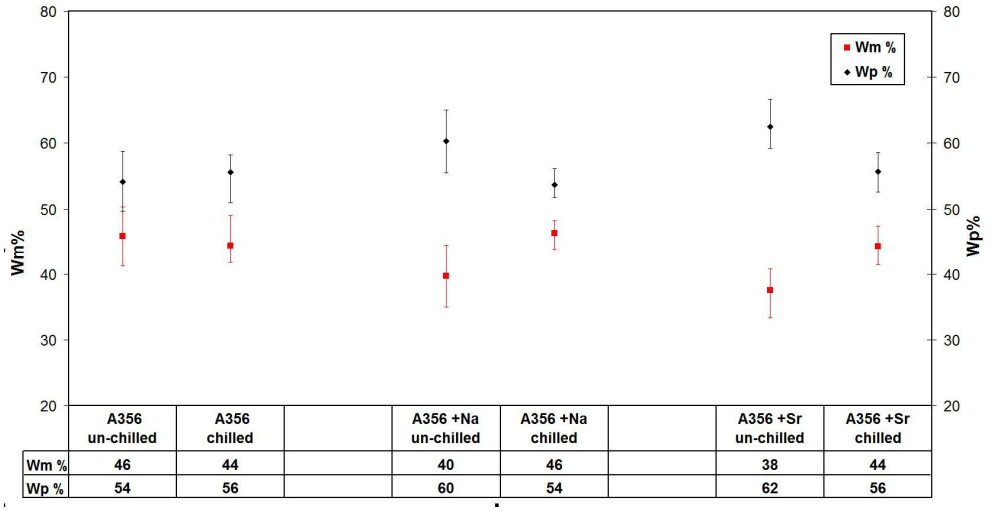

	A356 un-chilled	A356 chilled		A356 +Na un-chilled	A356 +Na chilled		A356 +Sr un-chilled	A356 +Sr chilled
Wm %	46	44		40	46		38	44
Wp %	54	56		60	54		62	56

Fig. 13. Percentage of nucleation and propagation energies for the three different alloys under the two different cooling conditions. Deviations from average values are shown as error bars.

The ductility of the alloy also depends on the size and morphology of eutectic silicon particles. In sodium-modified and strontium-modified alloys the eutectic silicon morphology changes from acicular to fibrous and therefore the ductility increases. As previously specified in section 3.2, the eutectic silicon distribution is less uniform in sodium-modified

samples than in strontium-modified ones and this confirms the lower percentage of the propagation energy in sodium-modified samples.

3.4. SDAS and impact strength relationship

SDAS measurements, evaluated by using the linear intercept method over the surfaces of the samples, have been correlated to impact energy values in order to investigate the microstructural effect on impact properties. SDAS values, the total impact energies, the propagation energies as a percentage of the total absorbed energies and solidification times are reported in Table 2. The SDAS values are in good agreement with the solidification times evaluated by thermocouples. There is an inverse correlation between SDAS and impact energy values: a small SDAS leads to an improvement in impact strength. By comparing the propagation energy of the modified alloys with SDAS values, a direct correlation can be found. As specified in the previous section, the data scatter for the unmodified alloy is too great to derive any clear correlation.

Table 2. Average SDAS and impact energy values. Solidification times are also reported.

	A356		**A356 + Na**		**A356 + Sr**	
	un-chilled	**chilled**	**un-chilled**	**chilled**	**un-chilled**	**chilled**
SDAS [µm]	81	30	79	30	81	30
Wt [J]	0.922	2.397	1.796	3.679	1.165	2.414
Wp%	54	56	62	56	60	54
Solidification time [s]	396	22	447	31	473	34

3.5. SEM analysis

The fracture surfaces of the samples have been examined by SEM in order to determine the effect of modification and the cooling rate on fracture behavior. In Fig. 14a the fracture surface of a sample of the unmodified and un-chilled casting reveals a transcrystalline fracture of a high-developed surface; regions of cleavage facets are present due to the presence of lamellar silicon particles and brittle intermetallic phases [9]. As can be seen in Fig. 14b, the presence of chills during solidification produces a finer microstructure; the fracture is still transcrystalline and secondary cracks are visible on the silicon particles.

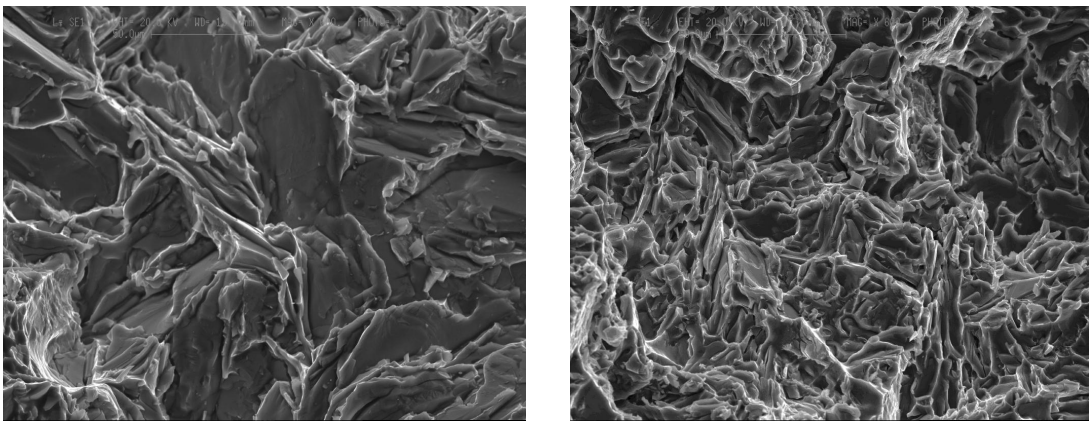

(a) (b)

Fig. 14. Features of the surface fracture of samples drawn from unmodified plate castings: a) un-chilled sample - transcrystalline and ductile fracture, b) chilled sample - finer microstructure, secondary cracks on silicon particles.

The presence of shrinkage porosity and the interdendritic path of the crack are evident on the fracture surface of sodium-modified and strontium-modified samples; Fig. 15 reveals that the fracture profile follows the interdendritic eutectic zone. A modification treatment, with either sodium or strontium, could increase the hydrogen content of a liquid alloy and as a result the formation of microporosities [10].

Precipitates of secondary phases are evident inside the shrinkage porosities on the fracture surface. An example is depicted in Fig. 16 for a sample of strontium-modified plates, submitted to a high cooling rate. The EDS analysis revealed the presence of $Al_{15}(Mn,Fe)_3Si_2$ platelets. Precipitates of ß-Al_5FeSi have been found in other zones.

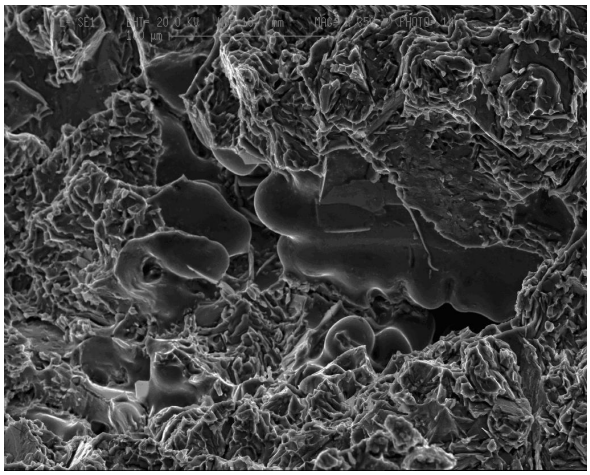

Fig. 15. Interdendritic path of the crack in a sample of strontium-modified plate.

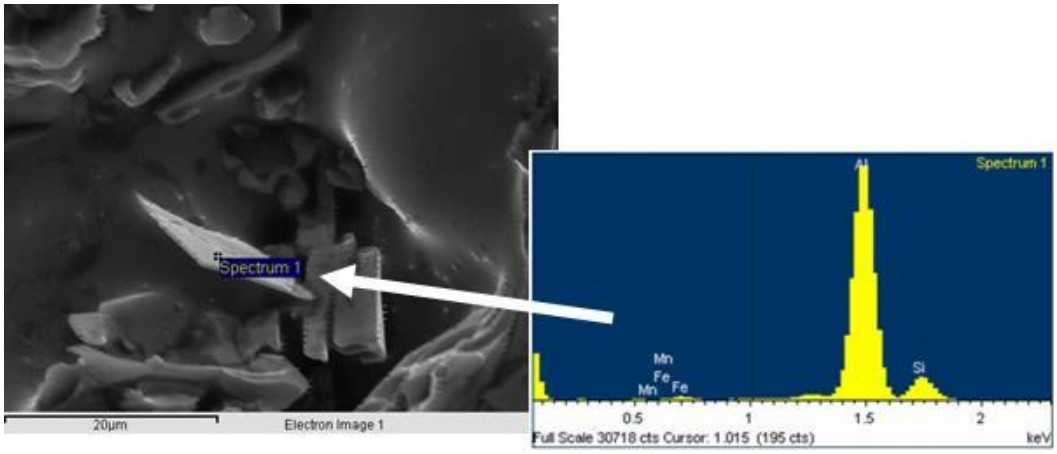

Fig. 16. SEM micrograph of $Al_{15}(Mn,Fe)_3Si_2$ platelet, with EDS spectrum.

3.6. Numerical simulation results

An important requirement for a good quality aluminum casting component is the optimal die filling, avoiding turbulence of the melt inside the mould cavity. The flow speed should be low in order to avoid oxidation of the melt and air entrapment: impact properties are negatively influenced by the presence of defects. As previously indicated in section 2.2, the CAD model of the casting system, taken into account during the research process, has been designed and imported into ProCAST. The software provides several numerical tools of investigation. The filling of the die has been accurately analyzed and a melt velocity below 0.3 m/s has been verified; the effectiveness of the filter as a damper velocity, which moves from 0.75 m/s to 0.4 m/s, can be noted in Fig. 17a. A good compromise between laminar filling and decrease in melt temperature has been obtained.

The study of the localization of the unavoidable shrinkage porosity due to solidification has been performed; in Fig. 17b all porosity is concentrated outside the plate casting, foreseeing the absence of macroscopic defects in the impact test samples.

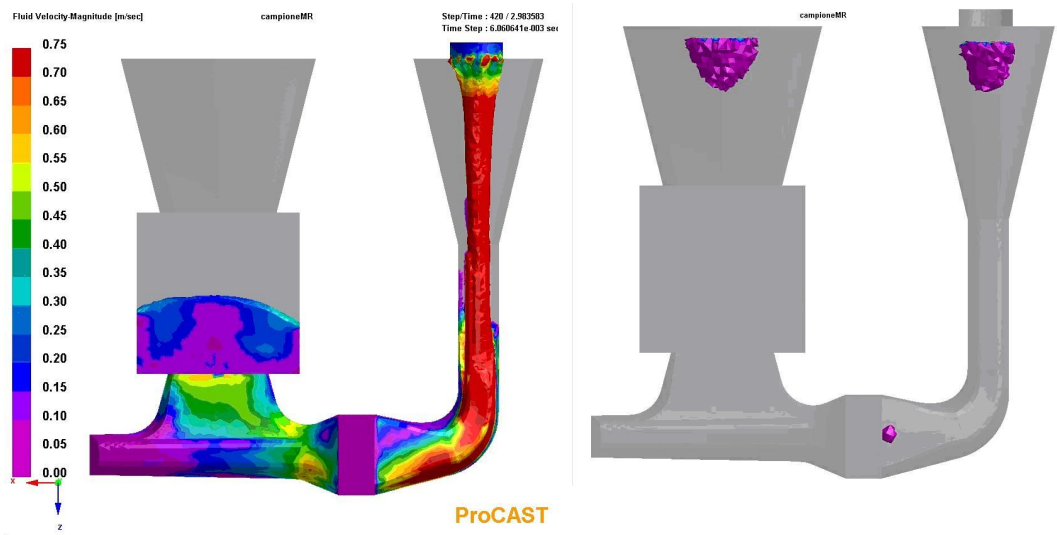

(a) (b)

Fig. 17. Features of the numerical simulations: a) filling of the die, with velocity estimate, b) porosity localization.

Fig. 18a and Fig. 18b show the SDAS values, calculated by means of numerical simulation; a significant difference between the two solidification rates can be observed. The average SDAS value in the un-chilled plates is about 31 μm and the standard deviation is very low. On the contrary in the chilled plates the average SDAS value is about 80 μm and the standard deviation is higher; this is in accordance with the higher standard deviations in impact energy results for chilled samples than for un-chilled samples. Moreover, by comparing Figs. 18a-18b and Table 2, it is interesting to note a good correspondence between average SDAS values, calculated by the numerical simulation code, and SDAS values acquired over the sample surfaces by using the linear intercept method.

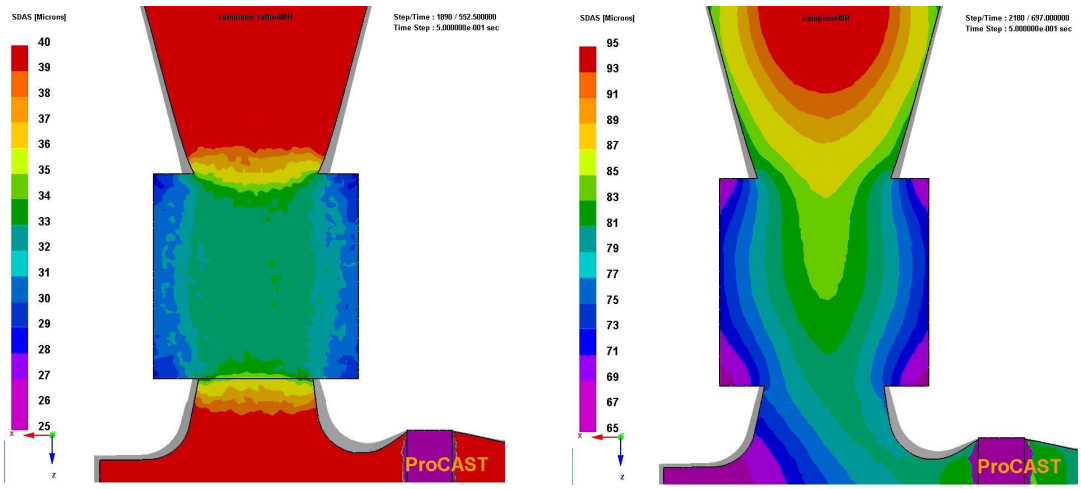

(a) (b)

Fig. 18. SDAS calculated with a numerical simulation approach: a) un-chilled plate casting, b) chilled plate casting.

4. CONCLUDING REMARKS

The following conclusions can be obtained regarding the influence of the microstructure on impact strength properties:

- The increase in the solidification rate determines a reduction in the SDAS values, and a finer microstructure always corresponds to a higher impact strength.
- Modified samples show higher impact strengths than unmodified ones; in particular, this is due to the change of eutectic silicon particles from acicular to fibrous morphology. This effect is emphasized in strontium-modified samples, where a more uniform distribution of eutectic silicon is found.
- A direct correlation between the propagation energy and SDAS is only obtained in modified samples, because the scatter of data is too large in unmodified ones.
- The fracture surface analysis reveals the interdendritic path of the crack, the presence of microshrinkage and of Fe-rich intermetallic platelets: $Al_{15}(Mn,Fe)_3Si_2$ and β-Al_5FeSi are identified by means of Energy Dispersive X-ray analysis.

Numerical simulations are useful when evaluating the quality of the casting as a result of the manufacturing cycle. They predict how the molten alloy fills the die cavity, the evolution of microstructure and the possible presence of defects. In this research a good correspondence between simulated and measured SDAS values has been found.

REFERENCES

1. Apelian, D., Shivkumar, S., and G. Sigworth. Fundamental Aspects of heat treatment of cast Al-Si-Mg alloys. *AFS Trans.*, 97 (1989), 727-742.

2. Li, Z., Samuel, A.M., Samuel, F.H., Ravindran, C., Doty, H.W., and S.Valtierra. Parameters controlling the performance of AA319-type alloys Part II. Impact properties and fractography. *Mater. Sci. Eng.*, A 367 (2004), 111-122.

3. Paray, F., Kulunk, B., and J.E. Gruzleski. Impact properties of Al-Si foundry alloys. *Int. J. Cast Met. Res.*, 13 (2000), 17-37.

4. Zhang, D.L., Zheng, L.H., and D.H. StJohn. Effect of a short solution treatment time on microstructure and mechanical properties of modified Al-7wt.%Si-0.3wt.%Mg alloy. *J. Light Met.*, 2 (2002), 27-36.

5. Shivkumar, S., Wang, L., and C. Keller. Impact properties of A356-T6 alloys. *Journal of Materials Engineering and Performance*, 3 (1994), 83-90.

6. Salem, S., Sjogren, T., and I.L. Svensson. Variations in microstructure and mechanical properties of cast aluminum EN AC 43100 alloy. *Metallurgical Science and Technology*, 25 N.1 (2007), 12-22.

7. Pedersen, L.. Solution heat treatment of AlSiMg foundry alloys, PhD thesis, Norwegian University of Science and Technology (NTNU), Trondheim, 1999.

8. Brown, R.. Foseco non-Ferrous foundryman's handbook. In Butterworth-Heinemann (Ed), Aluminium casting alloys, Oxford, 1999, pp. 23-45.

9. Warmuzek, M. Aluminium-Silicon Casting Alloys: Atlas of Microfractographs, In ASM International (Ed), 2004.

10. Gruzleski, J.E., and B.M. Closset. The treatment of liquid aluminum-silicon alloys. In American Foundrymen's Society Inc. (Ed), Modification and porosity, Des Plaines, Illinois, 1990, pp. 57-73.

Article 3

MECHANICAL AND MICROSTRUCTURAL CHARACTERIZATION OF A356 CASTINGS REALISED WITH FULL AND EMPTY CORES

Mattia Merlin*, Gian Luca Garagnani*

* Department of Engineering - ENDIF
University of Ferrara
I-44100 Ferrara
Italy

Metallurgical Science and Technology, (in press)

ABSTRACT

The use of full cores, for producing automotive components by means of the permanent mould casting technique, allows good castings with a low level of defects to be obtained. Nevertheless, an extra phase of the production cycle is necessary to have an optimal emptying of the internal cavities of the castings, with an increase in costs. This scenario motivated the present research, in particular to study the effect of replacing full cores with empty cores. The component analysed is one of the three parts of a motorcycle frame, realised in aluminum alloy A356 by permanent mould casting and T6 heat-treated. Several castings have been produced with both full and empty cores; tensile strength tests have been performed on samples drawn from four different zones, in order to compare the mechanical and microstructural properties of the castings realised with the two different kinds of core. A slight decrease in elongation at fracture has been verified in the samples drawn from the castings realised with empty cores, but yield strength and ultimate tensile strength are well comparable. A finer microstructure always corresponds to higher mechanical properties; an inverse correlation between secondary dendrite arm spacing and ultimate tensile strength has been found. The effect of secondary phases, porosities and morphology and distribution of eutectic silicon particles has been considered. The Japanese Taikai methodology has been improved in order to compare the current production cycle with the one optimised by the use of empty cores. Cost, weight and time-cycle reductions in the production of the component, due to the elimination of the extra phase using empty cores, have been evaluated.

Keywords

A356 alloy, permanent mould castings, sand cores, tensile properties, microstructure.

1. INTRODUCTION

In the automotive field the use of foundry aluminum alloys allows near-net-shape components to be produced, also for structural applications because of their high strength-to-weight ratio in heat-treated conditions. In particular, aluminum-silicon alloys have widespread applications in the field of transport because of their good castability, their corrosion resistance and their excellent recycling behaviour. Moreover, technological innovation and the increased usage of aluminum alloy could reduce emissions and energy consumption in the automotive sector. A better understanding of the relationship between microstructure and mechanical properties in cast aluminum-silicon alloys will improve foundry practice, in particular in those applications in which weight reduction is an important objective.

In their research, various authors report the effect of chemical composition and heat treatment on microstructure [1,2,3]. Also, analytical and empirical models correlating the main solidification parameters and the secondary dendrite arm spacing can be found in literature [4,5]. In A356 aluminum-silicon alloy, the secondary dendrite arm spacing (SDAS), the shape and distribution of eutectic silicon particles and secondary phases all control the tensile properties of pore-free castings [6]. The presence of Fe-rich secondary phases affects the mechanical properties of A356 alloy, in particular the ductility of the alloy. The amount and number of Fe-rich intermetallics strictly depend on the magnesium content [7,8]. Strontium additions and different solidification rates have a great effect on the microstructure; in cast aluminum alloys both yield strength (YS) and ductility are improved by the T6 heat treatment, due to the precipitation of fine β'-Mg_2Si particles and the spheroidisation of the eutectic silicon particles [9,10].

The aim of this study is to investigate the tensile properties of samples, drawn from several castings produced by the permanent mould casting technique. The component analysed is one of the three structural parts

of a motorcycle frame realised in strontium-modified A356 alloy. In current production, the cavities of the component are obtained by means of two full cores and bulges could develop on the surface of the component if, during the following T6 heat treatment, only a small quantity of sand is present. Generally, the mechanical vibration of the component at the exit of the cooling tunnel is not enough to completely eliminate the sand inside the internal cavities. Therefore, in order to avoid the presence of bulges, an extra phase in the production cycle – namely "hot flogging" - is necessary to completely empty the sand. Hot flogging determines an increase in the production costs of the component. The substitution of full cores with empty cores could eliminate the hot flogging phase. This way, less sand has to be eliminated and mechanical vibration is enough to completely empty the cavities in the component. Tensile strength tests have been performed on samples drawn from four different zones of several castings realised with full and empty cores in order to compare their mechanical properties, in terms of ultimate tensile strength (UTS), YS and percentage of elongation at fracture (A%). Microstructural features, such as SDAS and eutectic silicon particles, have been correlated to mechanical properties. In order to evaluate the presence of porosities in the castings and also in the samples, both macro and micro focus X-ray equipment have been used. In addition to metallographic inspections, fractographic analyses have also been performed on the fractured samples by means of Optical Microscopes (OM) and Scanning Electron Microscopes (SEM) with Energy Dispersive X-ray Spectroscopy (EDS), with the aim of determining SDAS, the presence of secondary phases, gas and shrinkage porosities, and of analysing the fracture profile and surface. The effect of microconstituents on crack nucleation and propagation has been evaluated. All mechanical and microstructural properties of the castings obtained with the two different kinds of core have been compared. The advantage of using

empty cores to reduce time and production costs has been quantified by means of the Japanese Taikai methodology.

2. EXPERIMENTAL

Research has been performed on experimental castings produced to optimise the properties of the rear component of a motorcycle frame – namely "rear-frame" - obtained by permanent mould casting and shown in Fig. 1. Tensile strength tests have been carried out on samples of several castings machined from four different zones, half realised with full cores and half realised with empty cores.

Fig. 1. Rear-frame (courtesy of TFC-Galileo).

2.1. Alloy and component production

The rear-frame castings have been produced with A356 alloy, whose wt.% chemical composition is shown in Table 1.

Table 1. Chemical composition of A356 alloy (typical range of element wt.%).

Alloy	Si	Fe	Cu	Mn	Mg	Zn	Sn	Ni	Al
A356	6.97 ÷ 7.38	0.086 ÷ 0.108	0.002 ÷ 0.003	0.003 ÷ 0.005	0.381 ÷ 0.425	0.006 ÷ 0.009	0.001 ÷ 0.002	0.004 ÷ 0.007	Bal.

The alloy has been melted in an electric-induction furnace at 740 ± 5°C, then modified by adding Al-10%Sr master alloy to achieve the target strontium level of 0.02 wt.%. The chemical composition of the alloy has been analysed by means of Optical Emission Spectroscopy (OES). The melt has been degassed with nitrogen for 20 minutes, using a rotary degasser before pouring. After solidification and mechanical vibration, only the castings with full cores have also been submitted to hot flogging, that is a solubilisation at 500°C for 480 minutes. Then the T6 heat treatment has been carried out on all castings, consisting of solubilisation at 530 ± 5°C for 6h, water quenching at 80 ± 5°C and artificially aging at 145 ± 5°C for 6h.

2.2. Cores production

The sand cores have been produced starting from granular sands covered by a thermoset resin. The shell moulding technique has been used for producing both full and empty cores; the sand has been blown on a metal model, pre-heated at 230°C in order to allow the polymerisation of the resin. The difference in producing the two types of core is found in the amount of time the sand remains in the metal mould. Sand cores are very expensive, so they have a great influence on the production costs. Empty cores in this case are on average 45% lighter than full cores, with advantages in terms of environmental impact and costs.

2.3. CNC measures

A tridimensional control unit has been used to measure all cores and castings and to verify their dimensional tolerances. The dimensions of the castings have been controlled after their solidification as they exit the cooling tunnel and also at the exit of the heat treatment plant; this way, possible differences with respect to nominal dimensions due to the heat treatment, are evaluated.

2.4. Tensile strength tests and non-destructive tests

Tensile samples have been machined from the castings in four different zones according to the Japanese norm JIS Z 2241:1998 “Method of tensile test method for metallic materials”. The dimensions of the samples are reported in Table 2. In Fig. 2, two of the four drawing positions of the samples have been highlighted. In order to distinguish between samples drawn from castings obtained by full cores and samples from empty cores, they have been named F_{xy}-samples and E_{xy}-samples, respectively. The subscript ‘x’ indicates the number of the casting and the subscript ‘y’ indicates the position, from 1 to 4. Tensile tests have been performed using an ITALSIGMA 20 kN testing machine and the mechanical properties have been measured according to UNI EN 10002-1:2004.

Table 2. Sample dimensions [mm].

	Over-all length	Thickness	Width of grip section	Gage length
Dimensions [mm]	60	2.5	8	25

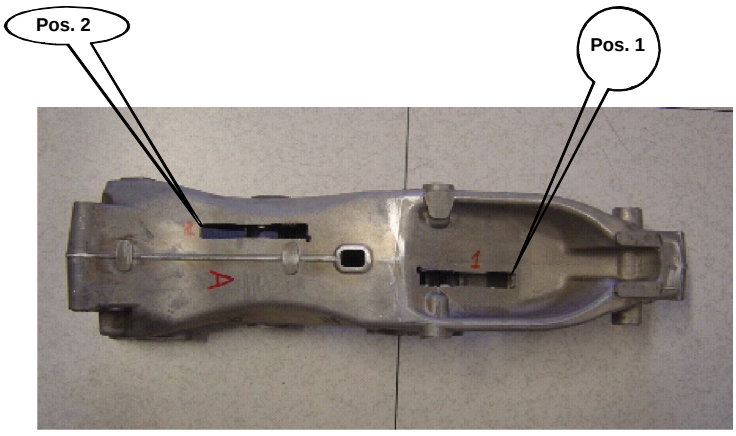

Fig. 2. The drawing positions 1 and 2 on the samples.

In order to verify the absence of macroscopic defects, macro focus X-ray equipment has been used for a preliminary analysis of the castings. Moreover, penetrating liquid tests have been carried out to control defects communicating with the external surfaces of the components. Also the tensile samples have been analysed by micro focus X-ray equipment, which can magnify an image several times offering more definition than a conventional X-ray tube.

2.5. Microstructural investigation

Microstructural analysis has been carried out on the tested fractured samples, using OM equipped with image analysis software. Average SDAS values have been obtained by means of the linear intercept method. In each specimen, ten random areas have been acquired over the entire surface and several measurements have been taken, in order to calculate mean values. The fracture profile has been observed on the prepared metallographic section, cut out perpendicularly to the fracture surface. Important information concerning the fracture mechanism and the microstructural components involved in the crack has been obtained. Also the effect of eutectic silicon particles and secondary phases has been evaluated.

The fracture surfaces have been examined using SEM and analysis of the main precipitates has been performed by EDS.

2.6. Taikai methodology

Taikai is a Japanese methodology that is useful in the evaluation of production cycles as it aims to increase the efficiency of the process according to the logic of continuous improvement. The method is composed of a series of phases. Some of these phases analyse the production layout and economical waste, others can define new improvement targets. The evaluation of the potential advantages, due to the substitution of full cores with empty cores in the production

cycle, has been carried out. In particular, the percentage reduction of weights, costs and the time-cycle has been calculated.

3. RESULTS AND DISCUSSION

3.1. Microstructural analysis

The microstructure of the components analysed consists of a primary phase, α-Al solid solution, and an eutectic mixture of aluminium and silicon. The primary phase precipitates from the liquid in the form of dendrites. The addition of strontium changes the eutectic silicon aspect ratio from acicular to fibrous. Fibrous eutectic silicon particles improve the mechanical properties of cast aluminium-silicon alloys [11]. The microstructure of the castings realised, by means of the two different kinds of core, has been compared in order to evaluate whether the different thickness of cores has a role in the microstructural and mechanical properties of the alloy.

3.1.1. Defects and secondary phases

Typical microstructures of samples drawn from the castings obtained by full and empty cores are reported in Fig. 3 and Fig. 4, respectively. Comparing Fig. 3a with Fig. 4a and Fig. 3b with Fig. 4b, SDAS values are in good agreement with the corresponding positions. The distribution of eutectic silicon particles is generally uniform and globular, as a consequence of the modification of the alloy and the heat treatment. Samples taken from positions 1 and 4 in castings obtained by means of empty cores show a distribution of eutectic silicon particles that is slightly less uniform than in the other positions.

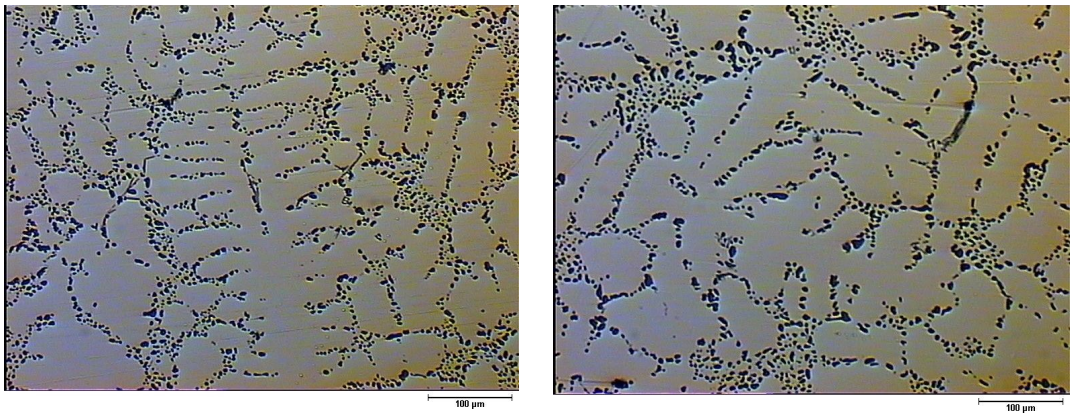

(a) (b)

Fig. 3. Microstructure of a casting realised with full cores: a) position 1, b) position 2.

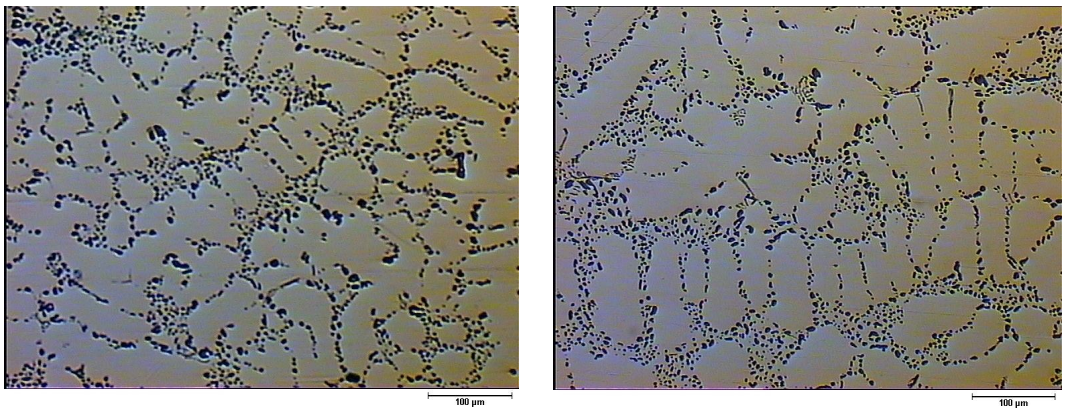

(a) (b)

Fig. 4. Microstructure of a casting realised with empty cores: a) position 1, b) position 2.

In aluminium-silicon alloys the loss of ductility, shock resistance and machinability is usually due to the presence of Fe [12]. As shown in Fig. 5, Fe-rich intermetallics with their typical needle shape and other secondary phase particles, such as α-Al(Mn,Fe)Si phase with the Chinese script morphology, have been observed in the specimens analysed [13]. Also microshrinkage and gas porosities have been found, in particular an interdendritic cavity is depicted in the micrograph in Fig. 6.

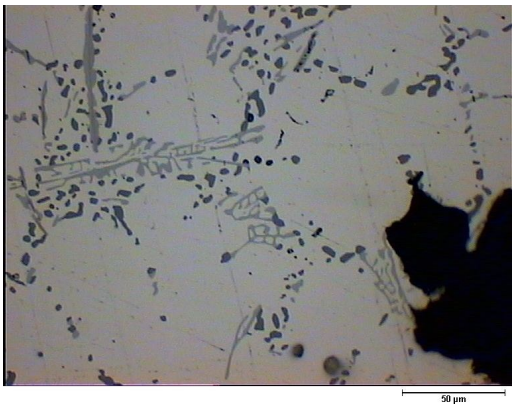

Fig. 5. Optical micrograph showing the presence of secondary phases.

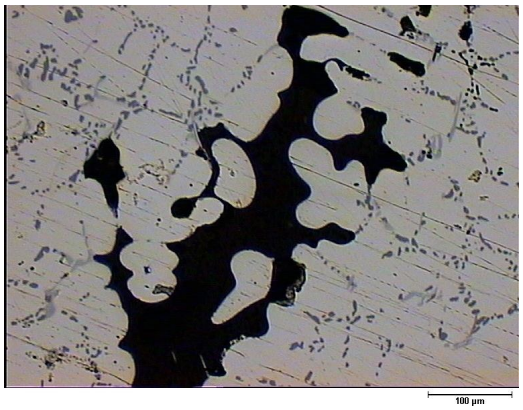

Fig. 6. Optical micrograph of shrinkage porosity.

3.1.2. Analysis of the fracture profile

Fracture profiles have been analysed by means of OM in order to understand the crack's growth and the effect of secondary phases better. As shown in Fig. 7, the crack crosses the interdendritic eutectic region where a significant fraction of intermetallics and eutectic silicon particles can be found. The presence of hard and needle-shaped phases determines high stress concentration. A large number of cracked silicon particles and secondary cracks parallel to the principal crack and normal to the tensile stress can be observed in Fig. 7 and Fig. 8.

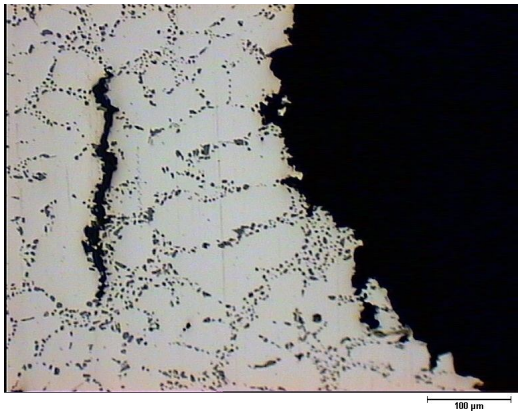

Fig. 7. Optical micrograph of the fracture profile: presence of a secondary crack.

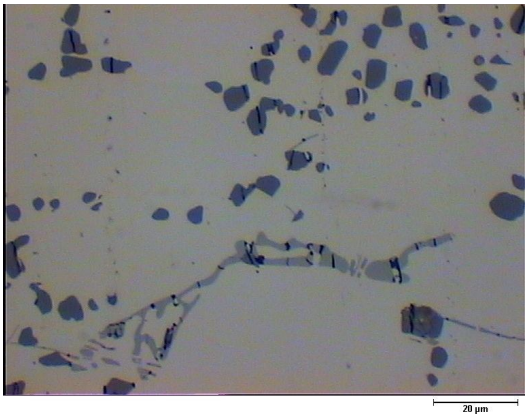

Fig. 8. Optical micrograph of cracked silicon particles and secondary phases.

3.1.3. SEM analysis of the fracture surfaces

As shown in Fig. 9, SEM analysis of the fracture surfaces of samples, taken from both types of casting, reveals a transcrystalline fracture [14]. This kind of fracture surface is typical of modified aluminum-silicon alloys subjected to T6 heat treatment. Visible traces of microdeformations (dimples) in the α-Al solid solution can be seen (Fig.10). In Fig. 11 the fracture surface reveals that dimples have been formed around cracked silicon particles, as a result of plastic deformation of the matrix. Fractures in the two-phase region with decohesion on the interface between α-Al and silicon particles have been found.

In Fig. 12 the presence of shrinkage porosity on the fracture surface is shown. The path of the crack is interdendritic, i.e. the fracture profile follows the interdendritic eutectic zone. Gas porosities have also been observed; the addition of either sodium or strontium for the modification of the alloy could increase the hydrogen content and, as a result, the presence of gas porosities [15].

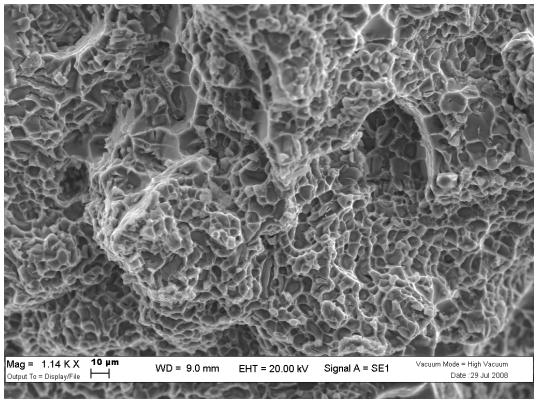

Fig. 9. Transcrystalline and ductile fracture.

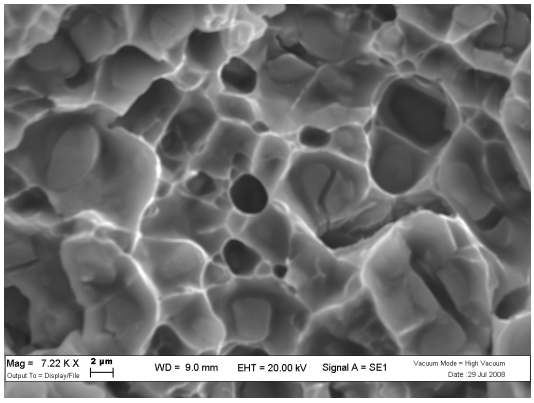

Fig. 10. Microdeformations in the α-Al solid solution.

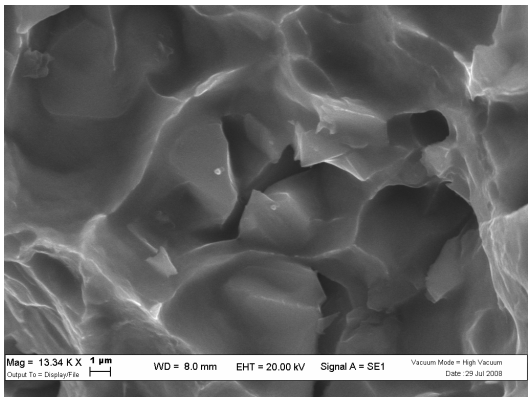

Fig. 11. Presence of a cracked silicon particle.

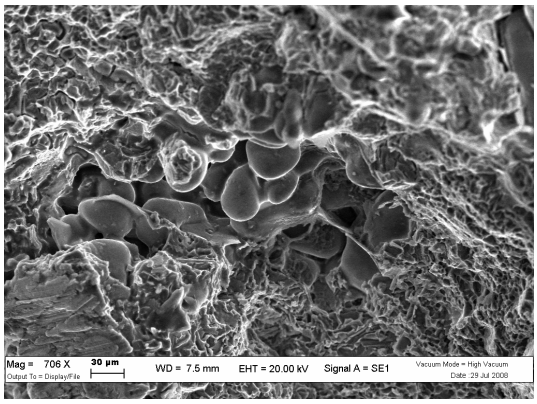

Fig. 12. Shrinkage porosity and the interdendritic path of the crack.

On the fracture surface and in particular inside the shrinkage porosities, the presence of secondary-phase precipitates has been observed. Both ß-(AlFeSi) and Al(Mg,Fe)Si intermetallic phases have been revealed by EDS microprobe. In Fig. 13 the SEM micrograph of a $Al_8Mg_3FeSi_6$ platelet with its EDS spectrum is reported.

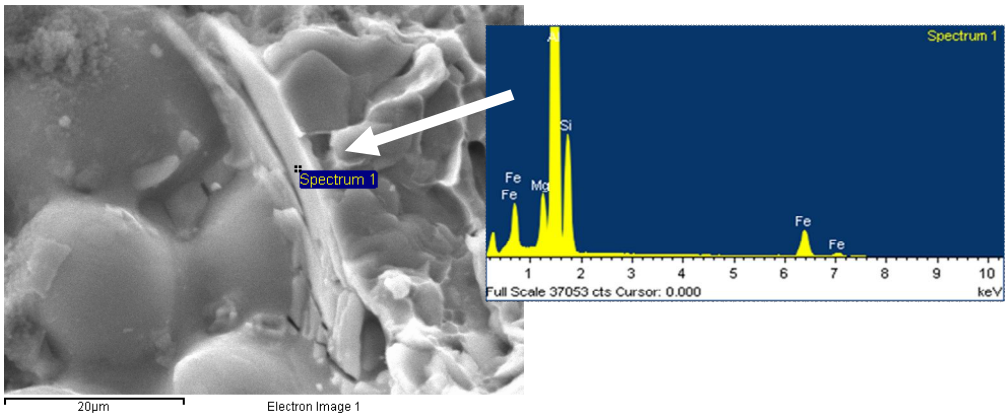

Fig. 13. $Al_8Mg_3FeSi_6$ platelet with its EDS spectrum.

3.2. Tensile testing results

From tensile tests, stress-strain curves have been obtained by attaching a knife-edge extensometer to the gage length. In Fig. 14 and Fig. 15 the mean values of UTS and of YS are shown, which have been

obtained from the samples drawn in the four different positions. The standard deviations are reported as error bars. UTSs in position 2 and position 3 show the highest values, but in all the four regions values are acceptable according to the expected range of values. Regardless of the drawing position, the samples machined from the castings obtained by empty cores (E_{xy}-samples) show higher YSs than the ones obtained by full cores (F_{xy}-samples). Notwithstanding, the maximum standard deviations of F_{xy}-samples are higher with respect to standard deviations of E_{xy}-samples.

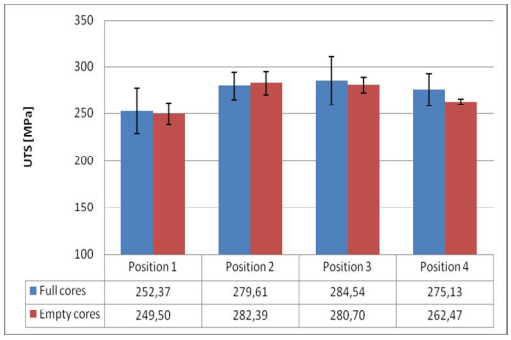

Fig. 14. Mean values of UTSs. The standard deviations are reported as error bars.

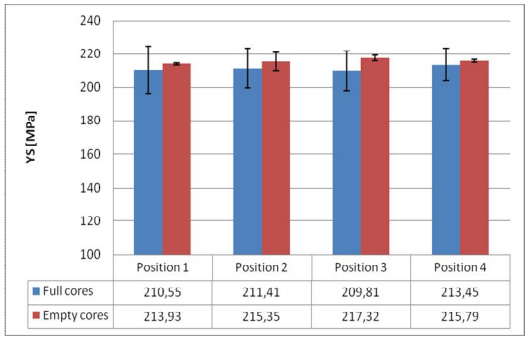

Fig. 15. Mean values of YSs. The standard deviations are reported as error bars.

In Fig. 16 the mean values of A% calculated on all samples are reported. The standard deviations are very high and only the castings obtained by means of full cores are within the project specifications. The lowest values in E_{xy}-samples are probably due to the elimination of the hot flogging phase in the production cycle. Castings realised by means of empty cores most likely need improvement in the heat treatment parameters, in order to increase ductility. Despite this lower A% in E_{xy}-samples, from data obtained from tensile tests, it is possible to conclude that the mechanical properties are comparable between the two different kinds of casting. Also, microstructural analysis has confirmed the main results obtained from mechanical tests. The

ductility of the alloy strongly depends on the size, morphology and distribution of eutectic silicon particles. In E_{xy}-samples drawn from position 1 and 4, silicon particle distribution is less uniform than in the other positions, and this confirms the lower mean values of A%.

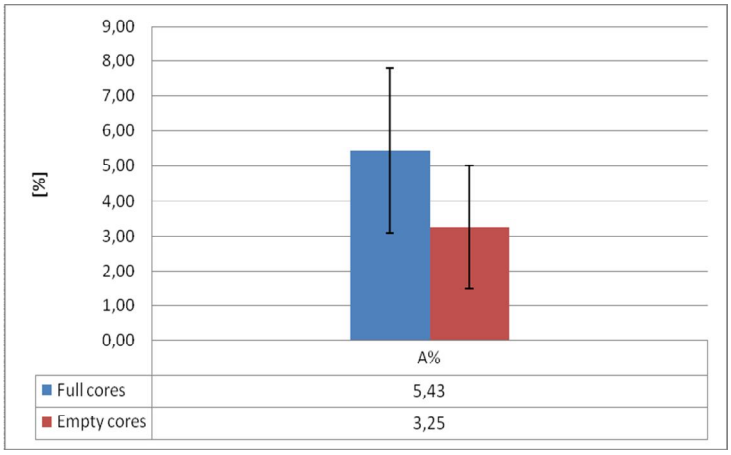

Fig. 16. Mean values of A%. The standard deviations are reported as error bars.

3.2.1. Relationship between tensile properties and SDAS

In Fig. 17 the SDAS mean values measured on F_{xy}-samples and E_{xy}-samples in the four different positions, are reported; as shown in the diagram, position 1 and 4 present the highest values and no significant differences among F_{xy}-samples and E_{xy}-samples SDAS values can be found in the different positions.

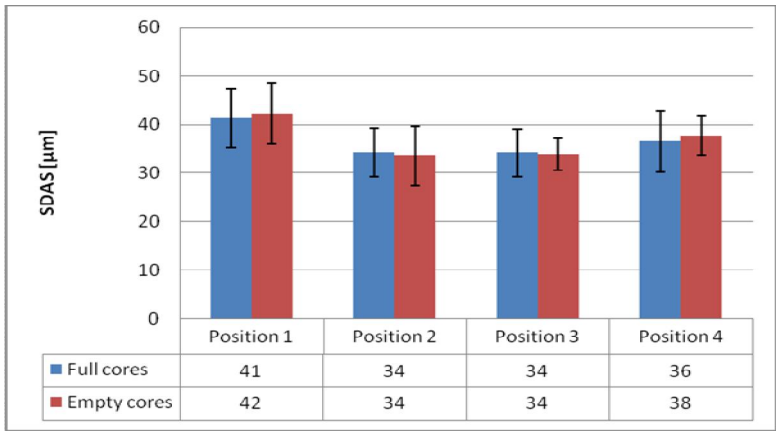

Fig. 17. Comparison of SDAS mean values in F_{xy}-samples and E_{xy}-samples. The standard deviations are reported as error bars.

The tensile properties of each sample, in particular UTS and YS, are plotted in Fig. 18 and Fig. 19 as a function of SDAS. SDAS measurements are correlated to tensile strengths with the aim of investigating the microstructural effect on mechanical properties. The results show that an inverse correlation between UTS and SDAS can be found for both F_{xy}-samples and E_{xy}-samples; a finer microstructure corresponds to a higher UTS. Unlike UTS, YS does not significantly depend on the scale of dendritic structure [6].

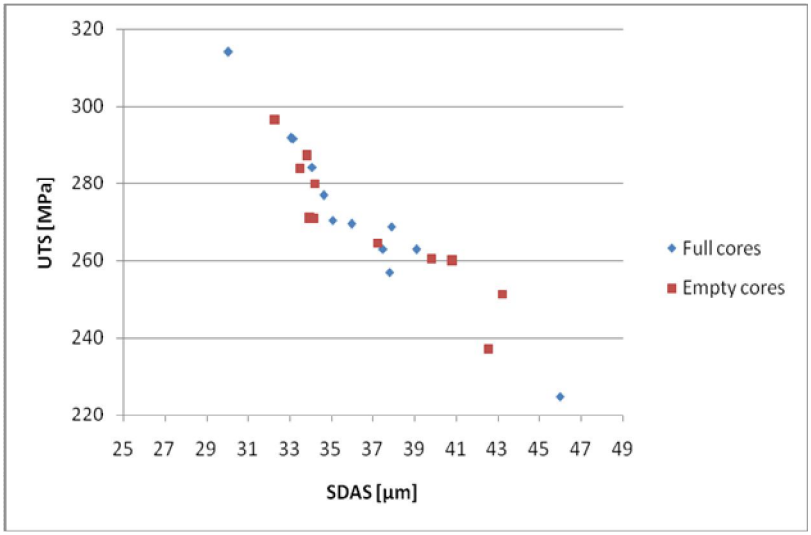

Fig. 18. Correlation between SDAS and UTS values.

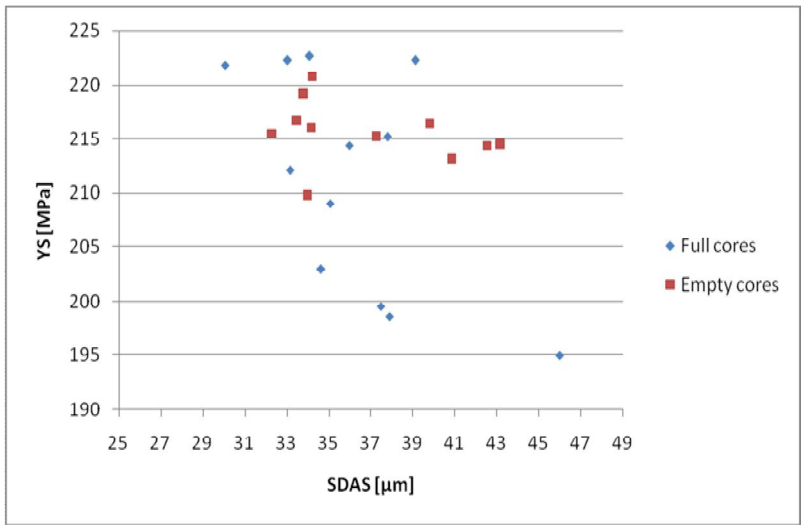

Fig. 19. Correlation between SDAS and YS values.

3.3. Taikai analysis

By means of Taikai methodology, the analysis of the potential advantages of substituting full cores with empty cores in the production cycle, has been carried out. In this analysis the reduction of weights, costs and time-cycle in the different phases of the production cycle with empty cores, with respect to the production cycle with full cores, has been evaluated. All this information is summarised in Fig. 20 and considerable advantages of using empty cores in the production cycle of the rear-frame component can be seen. In particular, the elimination of the hot flogging phase because of the use of empty cores determines a remarkable reduction in production costs. In Fig. 21 the total production costs have been compared; by means of Taikai methodology, a reduction of 9% in costs has been found when using the empty cores instead of using the more traditional full cores.

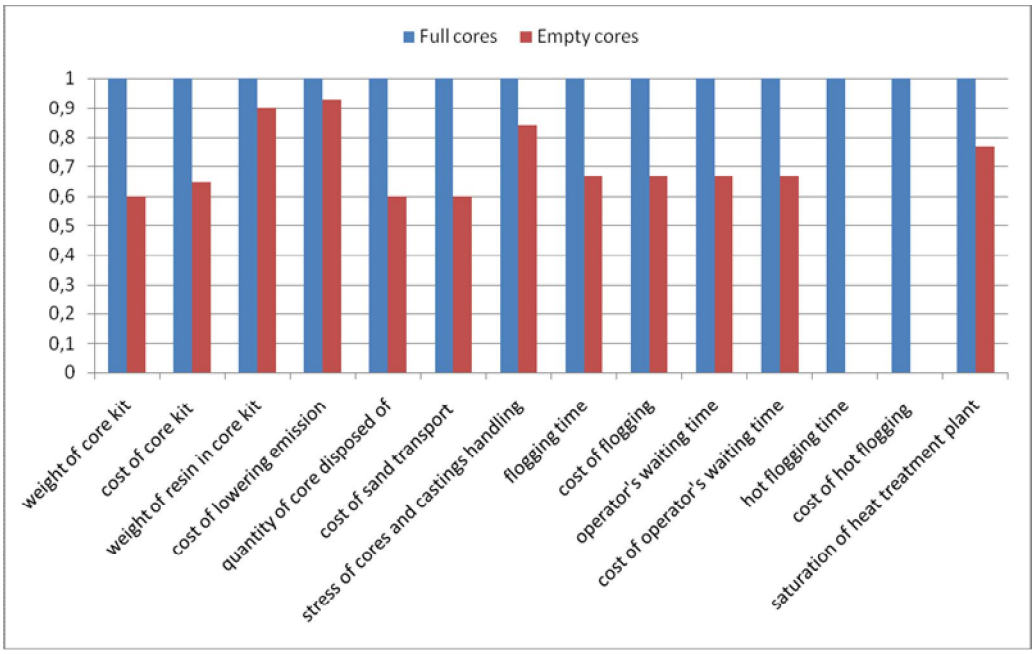

Fig. 20. Comparison of weights, times and costs of production with empty and full cores: normalised values.

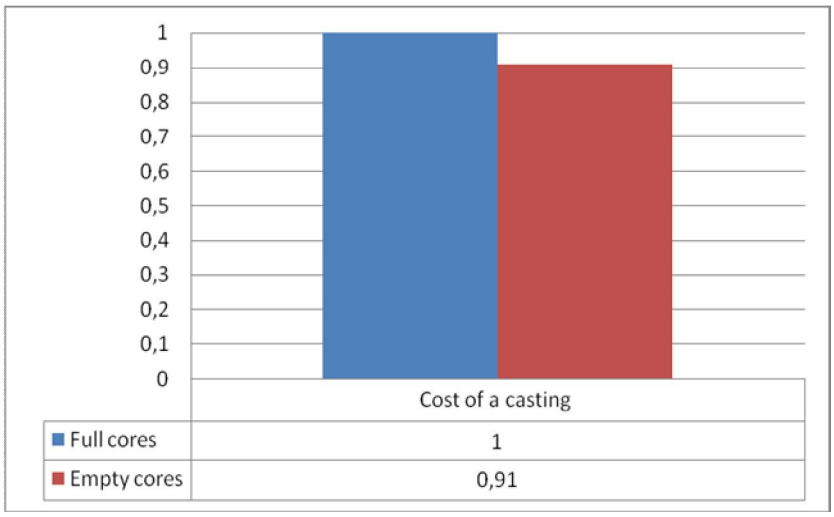

Fig. 21. Comparison of production costs with empty and full cores: normalised values.

4. CONCLUDING REMARKS

Tensile tests have been performed on samples drawn from four different positions of experimental castings of a motorcycle component, realised by permanent mould casting in aluminium-silicon A356 alloy and T6 heat-treated. Castings have been obtained by means of full sand cores, according to the current production cycle of the component, while other castings have been realised with empty sand cores. The aim of this research was to verify if the castings are comparable concerning mechanical and microstructural properties, and to evaluate the economical advantages of substituting full cores with empty cores.

The following conclusions can be obtained from the analysis of microstructure and mechanical properties of the castings, realised with full and empty cores:

- Secondary dendrite arm spacing is comparable in corresponding positions for the two kinds of castings. The distribution of eutectic silicon particles is generally uniform and globular.
- On average, UTSs and YSs are inside the expected range of values; A%s should be increased in the castings realised with empty cores, probably by means of an optimisation of the heat treatment parameters. In general the mechanical properties of both kinds of castings are comparable.
- An inverse correlation between UTS and SDAS is obtained; a finer microstructure always corresponds to higher UTSs. YS does not seem to be well correlated to the scale of the dendritic structure.
- The crack crosses the interdendritic eutectic region: cracked eutectic silicon particles and microshrinkage and gas porosities can be seen on the fracture surfaces. Also brittle intermetallic particles are identified by means of EDS analysis.

The results obtained by using the Taikai methodology reveal that several advantages from the use of empty cores instead of full cores can be obtained. In particular, a reduction in the weight of cores determines lower handling costs, lower emission costs and a lower

quantity of sand to dispose of. Moreover, the hot flogging treatment is not necessary to guarantee the required mechanical and microstructural properties and can be eliminated. Altogether, a reduction of 9% in the total production costs is evaluated.

ACKNOWLEDGMENTS

Many thanks are due to TFC-Galileo in Vaccolino of Lagosanto (Ferrara – Italy), for active cooperation and for supplying aluminum castings and X-ray equipment. The authors also express their gratitude to Dr. Stefano Succi for his experimental contribution to this research.

REFERENCES

1. Apelian, D., Shivkumar, S., and G. Sigworth. Fundamental aspects of heat treatment of cast Al-Si-Mg alloys. *AFS Trans.*, 97 (1989), 727-742.

2. Shan, Z., and A.M. Gokhale. Micromechanics of complex three-dimensional microstructures. *Acta Mater.*, 49 (2001), 2001-2015.

3. Merlin, M., and al. Impact behavior of A356 alloy for low pressure die casting automotive wheels, *Journal of Material Processing technology*, 209 (2009), 1060-1073.

4. Flemings, M.C.. *Solidification Processing*, In McGraw-Hill (Ed.), New York, (1974).

5. Spear, R.E., and G.R. Gardner. Dendrite cell size. *AFS Trans.*, 71 (1963), 209-215.

6. Wang, Q.C.. Microstructural effects on the tensile and fracture behavior of aluminum casting alloys. *Metallurgical and Materials Transaction A*, 34A (2003), 2887-2899.

7. Couture, A.. Iron in aluminum casting alloys – A literature survey. *AFS Int. Cast Met. J.*, 6 (1981), 9-17.

8. Càceres, C.H., Davidson, C.J., Griffiths, J.R., and Q.C. Wang. The effect of Mg on the microstructure and mechanical behavior of Al-Si-Mg casting alloys. *Metall. Mater. Trans. A*, 30A (1999), 2611-2618.

9. Paray, F., Kulunk, B., and J.E. Gruzleski. Impact properties of Al-Si foundry alloys. *Int. J. Cast Met. Res.*, 13 (2000), 17-37.

10. Zhang, D.L., Zheng, L.H., and D.H. St John. Effect of a short solution treatment time on microstructure and mechanical

properties of modified Al–7 wt.% Si–0.3 wt.% Mg alloy. *J. Light Met.*, 2 (2002), 27-36.

11. Pedersen, L.. Solution heat treatment of AlSiMg foundry alloys, PhD thesis, Norwegian University of Science and Technology (NTNU), Trondheim, (1999).

12. Brown, R.. Foseco non-Ferrous foundryman's handbook. In Butterworth-Heinemann (Ed), Aluminium casting alloys, Oxford, (1999), 23-45.

13. Salem, S., Sjogren, T., and I.L. Svensson. Variations in microstructure and mechanical properties of cast aluminum EN AC 43100 alloy. *Metallurgical Science and Technology*, 25 N.1 (2007), 12-22.

14. Warmuzek, M. Aluminium-Silicon Casting Alloys: Atlas of Microfractographs, In ASM International (Ed), (2004).

15. Gruzleski, J.E., and B.M. Closset. The treatment of liquid aluminum-silicon alloys. In American Foundrymen's Society Inc. (Ed), Modification and porosity, Des Plaines, Illinois, (1990), 57-73.

Article 4

EFFECT OF SILICON PARTICLES AND ROUGHNESS ON THE SURFACE TREATMENTS OF CAST ALUMINUM ALLOYS

Sara Ferlini*, Alessandro Morri**, Elena Ferri*, Mattia Merlin***, Gianpaolo Giacomozzi****

*CERMET S.cons.r.l - Progetto CALL, I-40057 Cadriano di Granarolo (BO), Italy

**Department of Metal Science, Electrochemistry and Chemical Technology – SMETEC, University of Bologna, I-40100 Bologna, Italy

***Department of Engineering – ENDIF, University of Ferrara, I-44100 Ferrara, Italy

**** VARVEL S.p.A., I-40056 Crespellano (BO), Italy

Presented at 3rd International Conference High Tech Die Casting, Vicenza, Italy, September 21-22, 2006

ABSTRACT

Silicon aluminum alloys are widely used for cast aluminum components; silicon determines the presence of an eutectic microstructure, which affects the results of the anodizing surface treatment. In this study, the influence of silicon content, morphology and distribution of the eutectic phase on the anodizing process has been investigated. Commercial alloys designated as EN 42100, EN 43100 and EN 46100 have been used. In addition to the silicon effect, the influence of the surface finishing, in particular the development of the oxide and its properties, has been evaluated. Each sample has been characterized with roughness profiles before and after the anodizing process; then, microstructural characterization of the coatings has been performed by means of optical and scanning electron microscopes. It has been possible to observe the negative effect of the silicon particles on the characteristics of the anodic layer, which grows according to the increase in the silicon percentage and in the size of the eutectic silicon particles. Under the same operational conditions, morphology and quantity of surface eutectic silicon particles, the growth of the anodic layer varies remarkably according to the surface roughness: when the roughness increases, a film of non-homogeneous oxide develops.

Keywords

Aluminum alloy, anodizing, anodic oxide layer, silicon particle, roughness.

1. INTRODUCTION

The employment of aluminum alloys stands out in all transportation fields and it is becoming more and more widespread in the construction industry and furnishing accessories sector [1-2]. One of the main surface treatments that these alloys undergo is the anodizing process, an electrolytic process of which the main purpose is to protect metal from corrosion by forming a layer of superficial oxide. This protective layer is considerably affected by the elements present in the alloy, which can create secondary and tertiary phases. Not all the constituents of the aluminum alloys damage the oxide layer: series 3*xxx* (Al-Mn), 5*xxx* (Al-Mg), 6*xxx* (Al-Mg-Si) and 7*xxx* (Al-Zn) can usually be subjected to anodizing, while we encounter more problems with alloys commonly used for the production of components by casting processes, in particular series 3*xx.x* (Al-Si-Cu) and 4*xx.x* (Al-Si). Silicon is the principal alloying element of cast aluminum alloys for sand casting, shell casting and die casting. It is well-known that this element increases the castability, permitting to obtain components which have complex shapes, and furthermore, it has a grain-refining action [3-10]. Silicon is present in the aluminum solid solution with very low percentages (0.05%at. at 300°C), therefore the microstructure of alloys with high silicon content is composed of an α-Al primary phase and an eutectic mixture of aluminum and silicon; the eutectic region generally affects the growth of the anodized layer and causes remarkable modifications to the morphology and distribution of the pores present within it.

During the anodizing process, the aluminum matrix is dissolved by the electrolyte to create Al^{3+} ions that produce a layer of Al_2O_3 when they bind to the oxygen. Al_2O_3 forms a continuous oxide layer in contact with the base metal, known as the barrier layer, and a porous layer on the top of it. Moreover, with the usual process parameters the eutectic silicon particles are exposed and undergo very slow oxidation, and are incorporated into the anodic layer. When the anodizing time is

increased, the volumetric fraction of silicon within the anodic layer increases, with consequent closure or deviation of the pores that characterize it. For this reason the electrolyte access to the base of the pore decreases, inducing an increase in the current density and increasing the barrier layer.

In order to obtain an anodic film that guarantees resistance to corrosion, not being able to directly act on alloys composition, we can operate in such a way that the eutectic silicon does not deteriorate the oxide layer. To perform this, the microstructural parameters taken into consideration are the distribution and the size of the silicon particles. As highlighted in several studies [11-13], the eutectic mixture of aluminum and silicon solidifies at the boundaries of the α phase. The growth of the oxide film takes place by following the morphology of the α phase, since the primary aluminum dissolves at different speeds according to the grain size and the presence of the eutectic silicon. With small-size grains the silicon has also a small size; with diameters smaller than 5 µm, the eutectic silicon particles are incorporated into the anodic layer, which appears continuous. In particular, because of the presence of the Al-Si eutectic region, the interfaces between the oxide layer and the base metal become irregular; this phenomenon occurs because the presence of the eutectic silicon reduces the quantity of dissolved aluminum locally, reducing the oxide thickness. For those particles of which the diameters fall within the range of 5 to 20 µm, the anodic layer is still able to incorporate the silicon, but this induces important modifications to the oxidized film: the thickness is considerably reduced and the growth speed decreased. For silicon sizes larger than 20 µm, the dissolution speed of the primary aluminum around the particles decreases and metallic aluminum can be found near the particles incorporated into the anodic layer. Table 1 summarizes the appearance of the anodic layer according to the variations of the size of silicon particles.

Since the anodizing process is a galvanic process, the growth of the anodic layer, in particular its thickness, is also affected by the initial roughness of the component. For this reason, the study has also taken into consideration, in addition to the influence of the presence of Al-Si particles, the influence of the initial roughness of the surface on the anodic layer growth, to understand the entire process better.

Table 1. Appearance of the anodic layer in the presence of the secondary phase [12].

Dimensions of the eutectic Si particles	**x < 5 μm**	**5 μm <x< 20 μm**	**x > 20μm**
Anodic layer appearance	The layer is continuous and well-adherent; the particles are incorporated into the film, causing its undulating behaviour.	The layer is continuous but with irregular thickness; the particles are incorporated into the film.	The layer can be discontinuous; the particles cause clear damage to the film.

2. EXPERIMENTAL

2.1. Aluminum alloys

EN 42100 and EN 43100 alloy sand-cast samples and EN 46100 alloy die-cast samples have been studied. The chemical composition of the examined alloys is reported in Table 2.

Table 2. Aluminum alloys chemical composition.

Alloy	**Si**	**Fe**	**Cu**	**Mn**	**Mg**	**Ni**	**Zn**	**Ti**
42100	6.5÷7.5	<0.20	<0.10	<0.10	0.20÷0.40	<0.05	<0.10	0.15÷0.20
43100	8.5÷9.5	<0.70	<0.10	0.40÷0.60	0.30÷0.45	<0.20	<0.10	<0.15
46100	11.0÷12.5	<1.10	1.75÷2.5	<0.50	<0.30	<0.30	<1.50	<0.20

2.2. Roughness analysis

The surface roughness has been determined by means of the HOMMEL T2000 TURBO surface roughness tester by HOMMELWERKE, which uses the Hommelwerke TKL 300 gauge. R_a parameter (1) has been obtained, which is the arithmetic mean of all the profile ordinates, filtered from shape errors and undulations, in absolute value, within the l_m length measure, that in this case is 4.8 mm.

$$R_a = \frac{1}{l_m} \int_{x=0}^{x=l_m} |y| dx \quad (1)$$

EN ISO 4287 confers surface parameters that allow the surface characteristics to be defined in such a way that they can be measured and compared.

Surface roughness measurements have been performed before and after the anodizing process; in particular, each sample shows four faces with different R_a values. Fig. 1 schematizes the sample section, highlighting the surface finishing of each side. On two surfaces, the initial roughness obtained from the casting process has been maintained: for the 42100 alloy, R_a = 7 µm (b side) and R_a = 12.8 µm (d side); for the 43100 alloy R_a = 6.1 µm (b side) and R_a = 10.9 µm (d side); for the 46100 alloy R_a = 7.5 µm on both sides. The two remaining surfaces have been machined to obtain a resultant R_a equal to 0.3 ± 0.1 µm (a side) and 1.5 ± 0.3 µm (c side), respectively.

2.3. Anodizing process

The surfaces of the samples have been prepared, then subjected to the anodizing cycle: they have been degreased by ethanol wash and dried with warm air (at 50°C for 1 minute), and successively the ultrasound neutralization in HNO_3 1/1 v/v at room temperature for 1 minute has been executed. The anodizing process has been carried out in H_2SO_4 2

M at 20 ± 1°C with 16 V voltage for 60 minutes. The samples have then been washed in distilled water for 5 minutes and dried with warm air (at 50°C for 5 minutes).

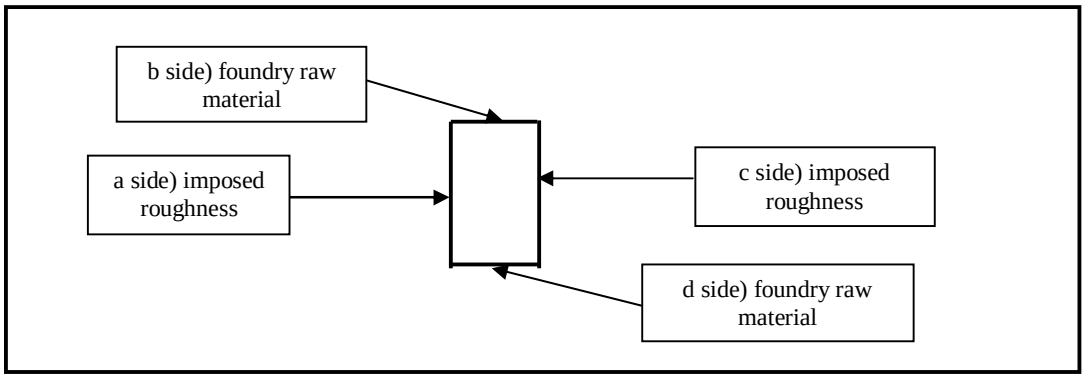

Fig. 1. Sample section with surface roughness indication.

2.4. Optical microscopy analysis

In order to examine the surfaces microstructure and oxide coatings, the samples have been cut by means of a micro-sprue cutter, embedded in epoxy resin and polished with STRUERS LaboPol-5 automatic system. No chemical etching has been executed.

The micrographs obtained have been subjected to image analysis, using IMAGE PRO Plus software, in order to determine the average thickness of the resulting oxide, and the size and shape of the eutectic silicon particles.

2.5. Scanning Electron Microscopy analysis

After removing the surface oxide, the test samples prepared for the metallographic analysis have been examined with a ZEISS EVO 50 scanning electron microscope in order to highlight both the substratum-oxide interface and the effects of the silicon particles on the development of the anodic film.

3. RESULTS

3.1. Roughness analysis

In the machined surfaces of the 42100 and 43100 alloys samples, where R_a was the lowest, we have observed an increase in the roughness levels after anodizing. This increase has not been observed for the 46100 alloy samples. In percentage, in the raw surfaces of both the sand-cast samples and the die-cast samples the roughness increase has been lower (Table 3).

The metallographic analysis has highlighted that the roughness variance of the machined surfaces is essentially associated to the presence in the anodic layer of the silicon particles, which differ in size and morphology according to the alloy and the casting process. Instead, the roughness increase in the raw surfaces is probably due to the fact that the presence of ridges and depressions determines a different growth speed of the anodic layer on the surface of the material.

Table 3. Roughness R_a (μm) before and after anodizing.

	Condition	a) side	b) side	c) side	d) side
42100	initial	0.4	7.0	1.2	12.8
	final	0.9	7.0	1.7	12.8
43100	initial	0.3	6.1	1.1	10.9
	final	1.0	7.7	1.3	14.6
46100	initial	0.3	7.5	1.5	-
	final	0.4	8.5	1.5	-

3.2. Metallographic analysis

The metallographic analysis of the samples has shown a remarkable difference of the oxide layers when the surface finishing varies. This aspect is especially evident in the 42100 and 43100 alloys, for which the sides characterized by low R_a have shown a more uniform anodic layer, compared to those with higher initial roughness. (Figs. 2-3). In the case of 46100 (Fig. 4), on the contrary, we can also observe a uniform anodic layer on the sides that have been left with the finishing derived from the casting process. The main effect of high roughness is the formation of surface depressions, within which the anodizing process continues in a preferential manner, pushing itself towards the inside of the piece. This creates an additional instability of the anodic layer, increasing the possibility that a detachment from the same piece occurs (Fig. 2-d).

This different aspect of the anodic layer on sand-cast and die-cast alloys is also linked to the different sizes of the eutectic silicon particles. In fact, in the presence of large size particles, the layer pattern is irregular and is full of cracks, while the presence of small size silicon particles assures a continuous and homogeneous anodic layer (Fig. 2-4). In the latter case, the particles are completely incorporated within the anodic layer. The results of the analysis of the eutectic silicon dimensions, reported in Table 4, have confirmed the above statement. The standard deviation values are due to the presence of both spherical silicon particles of small size and larger polygonal silicon particles.

In the 42100 and 43100 alloy samples, which have a non-uniform oxide layer, the silicon particles are coarse and have an elongated shape and their dimensions can be compared to those of the oxide layer itself. In the 46100 alloy the particles size is inferior by a factor of 4÷5 with respect to the anodized layer (Table 4). Consequently, they have a minor impact on the oxide film growth. This different morphology and dimension of the silicon particles are obviously due to both the

different casting process and the fact that the increase in silicon content in the alloy corresponds to an increase in the tendency of the particles to acquire a spheroid shape [14-17].

An evaluation of the anodic oxide thickness has also been performed, as shown in table 5. In the 42100 and 43100 alloy samples, the reduction of the surface roughness corresponds to an increase in the oxide layer thickness. Instead, at the same R_a the thickness of the anodic layer has a tendency to decrease when the silicon content in the alloy increases, regardless of the shape of the silicon particles. The data scattering is due to the irregularity of the anodic layer in proximity of the silicon particles.

The anodized thicknesses obtained with the 46100 alloy are significantly lower, since the high percentage of silicon in the alloy reduces the quantity of α phase on the surface of the sample. As mentioned above, the negative action of the silicon on the anodizing process takes place because, when increasing the silicon percentage in the alloy, the eutectic quantity on the surface also increases. In these conditions the eutectic α phase dissolves in a more difficult way, reducing the production of Al^{3+} ions that are necessary to build the layer. In spite of this, the film thickness is more homogeneous regardless of the initial roughness, due to the small dimensions of the eutectic silicon particles.

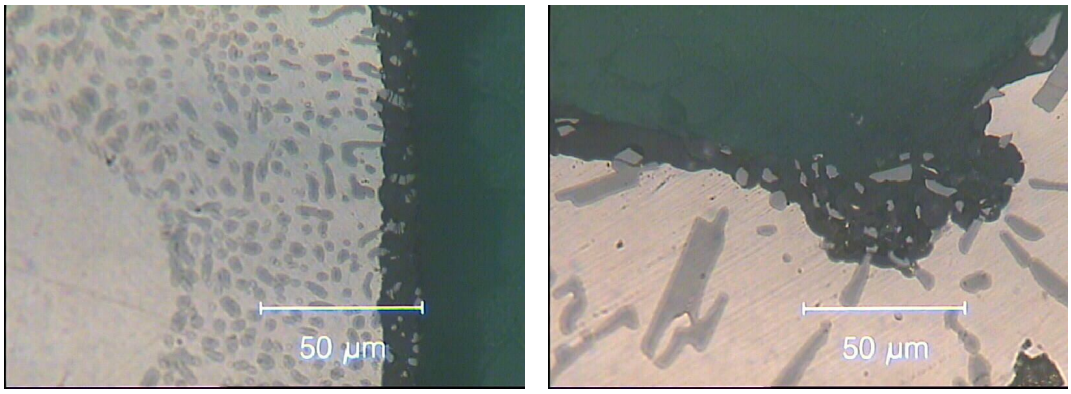

(a) (b)

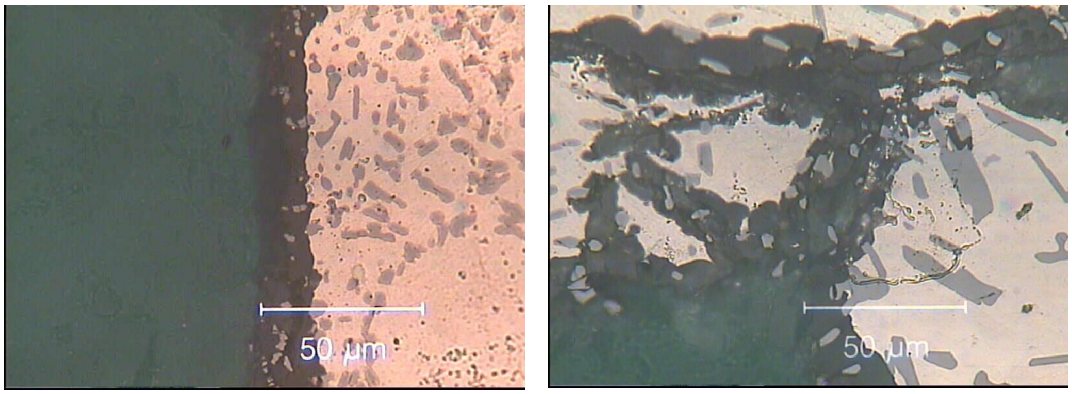

(c) (d)

Fig. 2. Optical micrographs of the anodized 42100 alloy; a) surface with initial R_a = 0.4 µm; b) surface with initial R_a = 7 µm; c) surface with initial R_a = 1.2 µm; d) surface with initial R_a = 12.8 µm.

Table 4. Dimensions of eutectic silicon particles.

42100		**Area (µm²)**	**(X) major axis (µm)**	**(x) minor axis (µm)**	**X/x**
	medium	32.7	8.4	4.0	2.1
	standard dev.	59.5	7.2	2.8	1.3
43100					
	medium	26.2	7.6	3.7	2.0
	standard dev.	41.0	5.7	2.1	1.0
46100					
	medium	1.2	1.6	0.9	1.9
	standard dev.	1.3	0.8	0.4	0.8

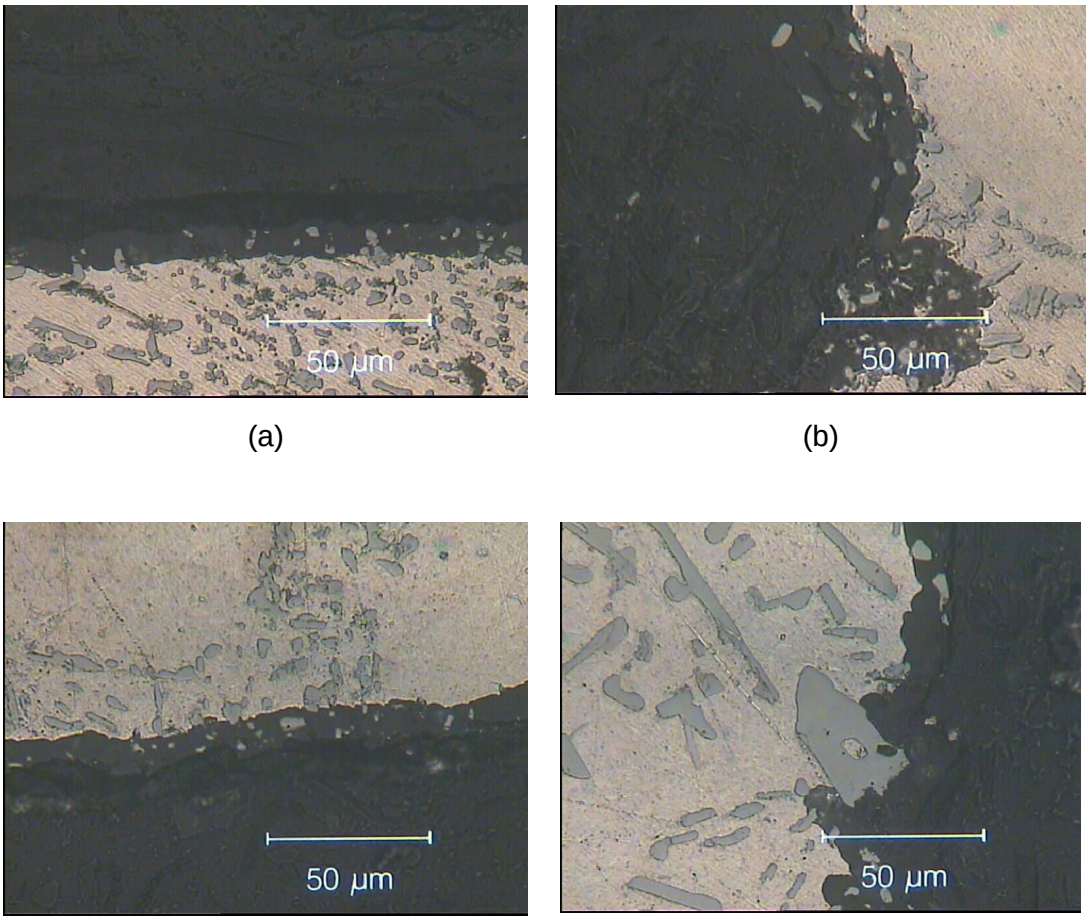

(a) (b)

(c) (d)

Fig. 3. Optical micrographs of the anodized 43100 alloy; a) surface with initial R_a = 0.3 µm; b) surface with initial R_a = 6.1 µm; c) surface with initial R_a = 1.1 µm; d) surface with initial R_a = 10.9 µm.

Table 5. Anodic oxide thickness expressed in µm according to the initial roughness.

42100		**a) side**	**b) side**	**c) side**	**d) side**
	medium	21.5	11.3	18.8	12.8
	standard dev.	5.7	5.1	5.1	3.9
43100					
	medium	17.3	14,0	18.3	13.4
	standard dev.	5.7	3.4	5.7	4.3
46100					
	medium	6.8	7.2	7.3	-
	standard dev.	2.3	1.8	2.6	-

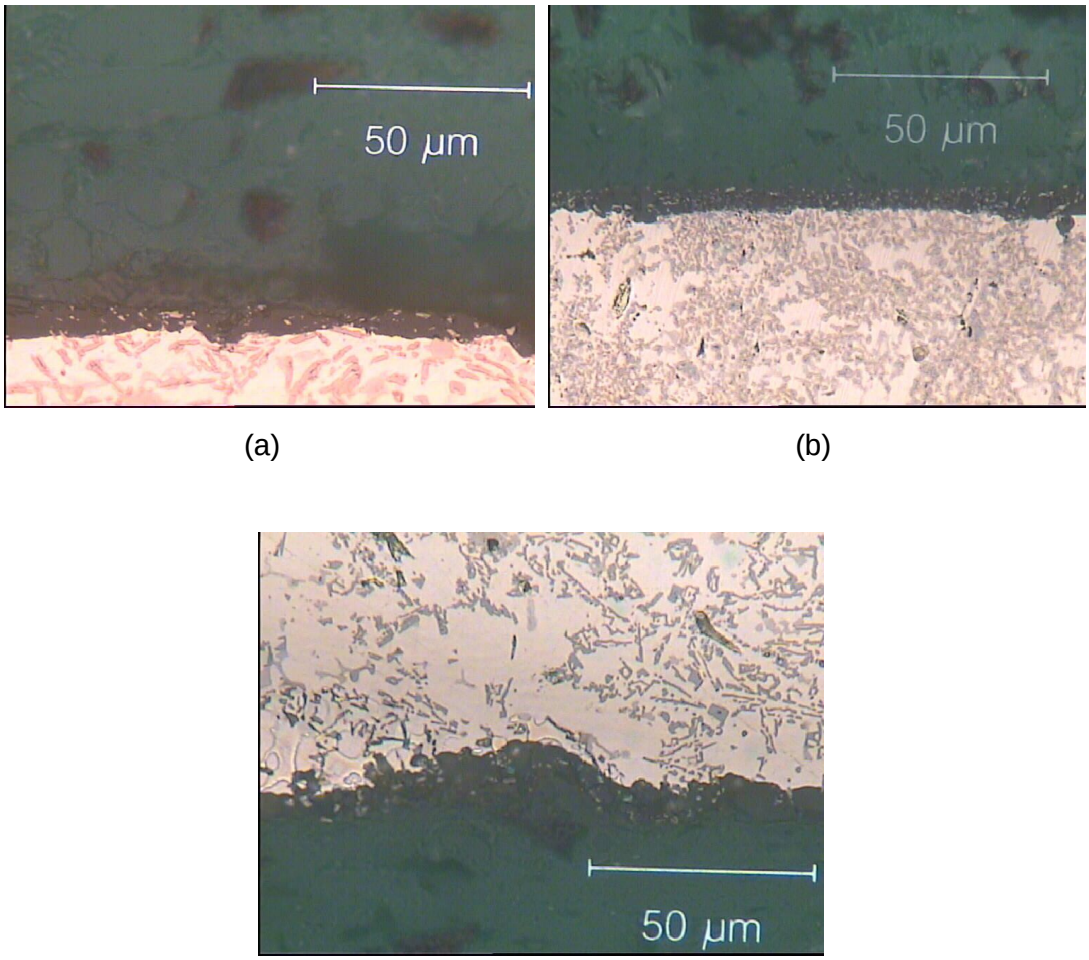

(a) (b)

(c)

Fig. 4. Optical micrographs of the anodized 46100 alloy; a) surface with initial R_a = 0.3 µm; b) surface with initial R_a = 7.5 µm; c) surface with initial R_a = 1.5 µm

3.3. Scanning Electron Microscopy analysis (SEM)

The optical microscopy analysis of 42100 and 43100 alloy samples has highlighted the damage to the anodic layer induced by the silicon particles. With regard to the 46100 alloy, the metallographic analysis has not shown any damage to the layer; this result has been confirmed by Scanning Electron Microscopy analysis (Fig. 5), which has shown an oxide layer well-adhered to the substratum. Furthermore, small size silicon particles have not determined anodic film decay, which appears

homogeneous and with uniform thickness, confirming that the shape and dimension of the eutectic silicon particles are determining factors in the formation of a continuous and adherent oxide layer.

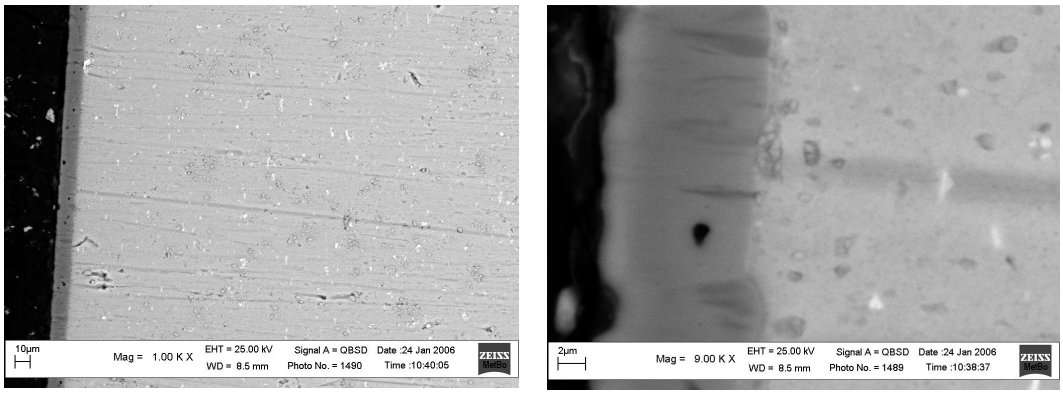

Fig. 5. Scanning Electron Microscopy analysis of the 46100 alloy after anodizing process at different magnification.

4. CONCLUSIONS

The effects of silicon and roughness on the 42100, 43100 and 46100 alloy samples, subjected to the anodizing process under the same process conditions, were investigated. Roughness measurements, optical microscopy analysis and scanning electron microscopy analysis have been executed.

- In the 42100 alloy, which has the lowest content of silicon among the alloys examined, the roughness increases after the anodizing process only for low R_a.
- For 43100 and 46100 alloys, where the percentage of silicon increases, the roughness values increase after the anodizing process for each level of examined R_a.
- Sand-cast samples show considerable differences between the oxide that formed on the machined sides (high thicknesses) and the one on the raw sides (low thicknesses), due to the surface irregularities.

- The oxide layer has homogeneous thickness in the die-cast 46100 alloy samples.
- The large size of the eutectic silicon particles present in the 42100 and 43100 alloy samples has contributed to the non-homogeneous oxide thickness, which is highly irregular and has cracks.
- Die-cast samples show silicon particles that are finely dispersed in the oxide layer; this does not cause lack of homogeneity in the film, even though it has a lower thickness.

ACKNOWLEDGEMENTS

Thanks to SMETEC Department of Metal Science, Electrochemistry and Chemical Technology of the University of Bologna, Italy, for the technical-scientific support. Thanks to VARVEL S.p.A. of Crespellano (Bo), Italy, for their availability and interest in scientific innovation.

REFERENCES

1. S. Ferlini, E. Ferri, ABDC 26 (2006) 56.

2. M. Toffolon, ABCD 24 (2005) 40.

3. I. Tsangaraki-Kaplanoglou, S. Theohari, Th. Dimogerontakis, Yar-Ming Wang, Hong-Hsiang Kuo, Sheila Kia, Surf. & Coat. Technol. 200 (2006) 2634.

4. F. Keller, M. Hunter, D. Robinson, J. Electrochem. Soc. 100 (1953) 411.

5. S. Wernick, R. Pinner, P.G. Seasby, The Surface Treatment and Finishing of Aluminum and its Alloys, vols. I, II, ASM International Finishing Publications LdT, England 1987.

6. H. Habazaki, et al., Corros. Sci. 39 (1997) 731.

7. H. Habazaki, K. Shimitzu, P. Skeldon, G.E. Thompson, G.C. Wood, Trans. IMF 75 (1) (1997) 18.

8. G.E. Thompson, H. Habazaki, K. Shimizu, M. Sakaizi, P. Skeldon, X. Zhou, G.C. Wood, Aircr. Eng. Aerosp. Technol. 71 (3) (1999) 228.

9. C.E. Caicedo-Martinez, G.E. Thompson, E.V. Koroleva, Surf. Eng. 18 (2002) 145.

10. C.E. Caicedo-Martinez, E.V. Koroleva, G.E. Thompson, P. Skeldon, K. Shimizu, H. Habazaki, G. Hoellrigl, Surf. Interface Anal. 34 (2002) 405.

11. L.E. Fratila-Apachitei, F.D. Tichelaar, G.E. Thompson, H. Terryn, P. Skeldon, J. Duszczyk, L. Katgerman, Electrochim. Acta 49 (2004) 3169.

12. L.E. Fratila-Apachitei, H. Terryn, P. Skeldon, G.E. Thompson, J. Duszczyk, L. Katgerman, Electrochim. Acta 49 (2004) 1127.

13. L.E. Fratila-Apachitei, J. Duszczyk, L. Katgerman, Surf. Coat. Technol. 157 (2002) 80.

14. X. Lui, G. Qi, X. Bian, Mater. Sci Forum 331-337 (2000) 367.

15. A.J. Griffin Jr., F.R. Brotzen, J. Electrochem. Soc. 141 (1994) 3473.

16. G.C. Wood, J.P. O'Sullivan, Electrochim. Acta 15 (1970) 1865.

17. G.E. Thompson, R.C. Furneaux, G.C. Wood, Trans. Inst. Metal Finish. 55 (1977) 117.